Engineering with Computers (2022) 38 (Suppl 1):S255–S276
https://doi.org/10.1007/s00366-020-01146-0

ORIGINAL ARTICLE

Pull-in and freestanding instability of actuated functionally graded nanobeams including surface and stiffening effects

Rasha M. Abo-Bakr[1] · Mohamed A. Eltaher[2,3] · Mohamed A. Attia[3]

Received: 29 May 2020 / Accepted: 11 August 2020 / Published online: 27 August 2020

Abstract
Because of fasttechnological development, electrostatic nanoactuator devices like nanosensors, nanoswitches, and nanoresonators are highly considered by scientific community. Thus, this article presents a new solution technique in solving highly nonlinear integro-differential equation governing electrically actuated nanobeams made of functionally graded material. The modified couple stress theory and Gurtin–Murdoch surface elasticity theory are coupled together to capture the size effects of the nanoscale thin beam in the context of Euler–Bernoulli beam theory. For accurate modelling, all the material properties of the bulk and surface continuums of the FG nanoactuator are varied continuously in thickness direction according to power law. The nonlinearity arising from the electrostatic actuation, fringing field, mid-plane stretching effect, axial residual stress, Casimir dispersion, and van der Waals forces are considered in mathematical formulation. The nonlinear nonclassical equilibrium equation of FG nanobeam-based actuators and associated boundary conditions are exactly derived using Hamilton principle. The new solution methodology is combined from three phases. The first phase applies Galerkin method to get an integro-algebraic equation. The second one employs particle swarm optimization method to approximate the integral terms (i.e. electrostatic force, fringing field, and intermolecular forces) to non-integral cubic algebraic equation. Then, solved the system easily in last phase. The resulting algebraic model provides means for obtaining critical deflection, pull-in voltage, detachment length, minimum gap, and freestanding effects. A reasonable agreement is found between the results obtained from the present method and those in the available literature. A parametric study is performed to investigate the effects of the gradient index, material length scale parameter, surface energy, intermolecular forces, initial gap, and beam length on the pull-in response and freestanding phenomena of fully clamped and cantilever FG nanoactuators.

Keywords Pull-in instability · Freestanding phenomenon · FG nanobeams · Modified couple stress theory · Surface energy · Galerkin method · Particle swarm optimization method

1 Introduction

Recent advances in the application of nanotechnology have resulted in the manufacture of nanoelectromechanical devices. The attractiveness of them is due to their excellent and distinctive mechanical and electrical properties, Ebrahimi and Hosseini [21]. Recently, FGMs are employed in micro/nano-electro-mechanical system (MEMS/NEMS) and atomic force microscopes (AFMs) to achieve high sensitivity and desired performance, [23, 24]. Electrostatic micro/nano-actuator devices like nanosensors, nanoswitches, and nanoresonators are widely used and can be modeled as nanobeam structures, Younis [81]. These devices usually comprise a conductive deformable body suspended above a rigid grounded body, Batra et al. [13]. When the applied voltage between the two bodies reaches an upper limit, called "pull-in voltage", they eventually collapse due to interaction between electrostatic and elastic forces. Accurate estimate of the pull-in voltage is crucial in the design of micro/nano-actuator devices. For a switching device, the designer exploits pull-in phenomenon to optimize device's

✉ Mohamed A. Eltaher
meltaher@kau.edu.sa; mmeltaher@zu.edu.eg

Mohamed A. Attia
madly@zu.edu.eg

[1] Mathematics Department, Faculty of Science, Zagazig University, Zagazig 44519, Egypt

[2] Mechanical Department, Faculty of Engineering, King Abdulaziz University, P.O. Box 80204, Jeddah, Saudi Arabia

[3] Mechanical Design and Production Department, Faculty of Engineering, Zagazig University, Zagazig 44519, Egypt

performance while for a micro-resonator, the designer avoids this phenomenon to achieve stable motion.

Rotation in continuum solid mechanics is divided into two kinds; one is independent called micro-polar rotation, which represents one sort of microstructure effects, and the other is the anti-symmetric part of displacement gradient field, called local rotation. In fact, the local rotation, at a point of the continuum, represents a constraint on the displacements at this point that induces an additional couple stress and, consequently, contributes on the strain energy density of the continuum. In the present study, the local-rotation is captured using the modified couple stress theory (MCST), Yang et al. [78]. For nanoscale structures, the surface is regarded as a membrane with a negligible thickness, [31, 32], where the atoms' arrangements and material properties differ from those of the bulk material. For nanostructures with higher ratio of surface layer volume to the bulk volume, surface energy effect becomes effective and cannot be ignored, Miller and Shenoy [43], and Shenoy [68].

Therefore, a nonclassical couple stress continuum model considering the effect of surface energy is proposed. In the present study, modified couple-stress theory and surface elasticity theory are exploited to develop an integrated model to investigate simultaneously the effects of microstructure local rotation and surface energy on the response of nano-devices. Using different beam theories in conjunction with combined influence of microstructure and surface energy, static and dynamic analyses of micro/nanoscale beams and plates have been investigated by some researchers, i.e. Gao and Mahmoud [29], Gao [28], Gao and Zhang [30], Shaat et al. [63], Zhang and Gao [86], Wang et al. [75], Attia and Mahmoud [5, 6], Attia et al. [10], and Shanab et al. [66, 67, 65].

In this regard, various experimental [12, 34], analytical [11, 55, 60, 59], [61, 14, 42, 47], and numerical [8, 2, 4, 6, 7, 55, 64, 88] investigations have been conducted on the pull-in instability behavior of micro/nano-beams subjected to electrostatic loadings. Numerical methods including finite difference method (FDM) [51, 55, 62], finite element method (FEM) [33, 45], differential quadrature method (DQM) [33, 74], [80], [4], and reduced order model (ROD) [14, 44, 54, 82] can predict the pull-in voltage with a very high degree of accuracy; however, these methods are computationally intensive.

Closed and semi-analytical expressions for pull-in voltages of micro/nano-actuators are very helpful since they save time and complex computational work required by numerical methods. Several researchers have provided closed-form expressions for the calculation of pull-in voltage [11, 42, 55]. Osterberg and Senturia [46] and Pamidighantam et al. [48] assumed a lumped spring mass model to obtain a closed-form expression for the pull-in voltage of microstructures such as beams/plates with different end conditions. Based on a lumped two degrees of freedom model, Bochobza-Degani and Nemirovsky [15] presented an analytical solution for calculating the pull-in parameters of electrostatic actuators. Baghani [11] presented an analytical solution for size-dependent response of cantilever micro-beams based on the MCST using the modified variational iteration method. Rokni et al. [55] derived analytical closed-form solutions in explicit forms for electrostatically actuated cantilever and fully clamped micro-beams based on the MCST. However, the solution of this approach is nontrivial. On the other hand, including nonlinearity caused by fringing field and/or intermolecular forces much complicates this approach. In Bhojawala and Vakharia [14], a closed-form for static pull-in voltage of fully clamped electrostatically actuated microbeam was derived as an explicit function of mid-plane stretching, axial load, fringing field, Casimir force, and finite conductivity. This closed form is invalid if other effects such as couple stress, surface residual stress, surface elasticity, van der Waals force, and/or material gradation are included. Miandoab et al. [42] predicted the static pull-in voltage of clamped-free, clamped–clamped and curved nanobeams based on the MCST, by transforming governing equations to a single degree of freedom model using Galerkin method and Genetic Algorithm to approximate the integral form of electrostatic force to non-integral form. However, this closed form does not account for fringing field or intermolecular forces.

In general, intermolecular forces are negligible for MEMS, where the separation distance is of the order of micron, but they play a significant role for NEMS, where the gap reduces to the nanoscale. Ramezani et al. [53, 52] obtained closed-form solutions for the pull-in parameters of cantilever nanoswitches subjected to intermolecular, electrostatic, and fringing forces using the Green's function. They estimated the detachment length and the minimum initial gap of freestanding nanocantilevers. Radi et al. [49, 50] investigated the pull-in instability of nanocantilevers actuated by electrostatic force and subject to Casimir or van der Waals forces by using the Green's function. This approach provided accurate predictions for the pull-in parameters of a freestanding nanoactuator. However, they did not consider the influences of microstructure, surface elasticity, and surface residual stresses parameters, which are important when the physical dimensions of structures descend to nanoscale. The influence of the surface energy on the pull-in instability of nanocantilevers under the electrostatic, fringing forces, and Casimir intermolecular attraction was investigated by Farrokhabadi et al. [26]. They employed the Duan–Rach method of determined coefficients and included the contribution of the surface energy on the free end boundary conditions, which have been ignored by almost other researchers.

Recently, Dehghan et al. [17] investigated the wave propagation analysis of fluid-conveying magneto-electro-elastic

nanotube incorporating nanoscale effect by using nonlocal elasticity theory of Eringen. Ebrahimi and Hosseini [20] studied analytically nonlinear vibration and dynamic instability of nonlocal nanobeams under thermo-magneto-mechanical loads by using Galerkin method and multiple scales method. Sahmani et al. [58] developed analytical solution for vibrational response of postbuckled laminated FG graphene platelet-reinforced composite nonlocal strain gradient nanobeams. Ebrahimi et al. [22] studied bending of magneto-electro-elastic analysis of piezoelectric–flexoelectric nonlocal nanobeams rested on silica aerogel foundation. Ebrahimi and Hosseini [21] presented effect of residual surface stress on nonlinear dynamics and instability of double-walled nanobeams by using nonlinear Mathieu–Hill equation. Wu and Liu [76] studied nonlinear thermo-mechanical response of temperature-dependent FG sandwich nonlocal strain gradient nanobeams with geometric imperfection. Xie et al. [77] investigated nonlinear secondary resonance of FG porous silicon nanobeams under periodic hard excitations based on surface elasticity theory. For more details, many recent studies in the literature on the static and dynamic response of nanobeams and nanoplates in the context of the nonlocal elasticity theory, nonlocal strain gradient theory, or modified couple stress theory have been developed, i.e. Fattahi et al. [27], Thanh et al. [71], Fan et al. [25], Ma et al. [40], Sahmani and Safaei [57], Trinh et al. [73], Yi et al. [79], Yuan et al. [85, 83, 84], Zhang and Liu [87], Lyu et al. [39], Liu et al. [38] and Liu and Lyu [37].

From the prementioned literature, it is noticed that the availability of closed-form or analytical model expressions for static pull-in instability analysis is still limited. These closed-form models mostly suffer from increased complexity and they may involve complicated mathematical operations. Therefore, the objective of the present paper was to propose a generalized closed-form expression for the size-dependent pull-in voltage of electro-mechanical FG nanobeams as well as the critical parameters of freestanding nanoactuator. The mathematical model is derived utilizing Hamilton principle taking into account the simultaneous effects of material length scale parameter, surface elasticity, and surface residual stress as well as nonlinearity raised by mid-plane stretching effect, axial residual stress, and van der Waals, Casimir, and electrostatic forces including fringing field under static condition in conjunction with Euler–Bernoulli beam theory. Power law distribution is employed to describe the material distribution of bulk and surface continuums through thickness and consequently the physical neutral axis is considered. Application of Galerkin method transforms the highly nonlinear integro-differential governing equation into a highly nonlinear integro-algebraic equation. The main idea behind the proposed closed-form solution is to replace appropriately the integral-terms in this equation by non-integral algebraic functions with undetermined coefficients. Particle Swarm Optimization (PSO) method is utilized to determine these coefficients such that they minimize the error between integral- and non-integral forms. Based on the resulting algebraic equation, generalized simple closed forms for the pull-in voltage and freestanding parameters are derived.

Accordingly, the present paper was organized as follows: in Sect. 2, the size-dependent governing equation and associated boundary conditions are derived. Section 3 presents the proposed solution method and its accuracy is verified by comparing the obtained results with other reported literature in Sect. 4. Section 5 presents an extensive parametric study to explore the effects of various material and geometrical parameters on the pull-in response as well as proposed expressions for permissible detachment length, minimum gap, and pull-in parameter parameters. Finally, Sect. 6 presents conclusion including key findings.

2 Theoretical formulation

An electrostatically actuated FG nanobeam is depicted in a rectangular coordinate system as illustrated in Fig. 1. The beam has length L with a uniform rectangular cross section of width b and thickness h. The initial gap separating the nanobeam from the substrate is d. The effective material properties $\mathcal{P}$ of the FG nanobeam that vary continuously along the thickness are described according to the following power law:

$$\mathcal{P}(z) = \left(\mathcal{P}_U - \mathcal{P}_L\right)\left(\frac{1}{2} + \frac{z_{\mathrm{m}}}{h}\right)^k + \mathcal{P}_L, -\frac{h}{2} \le z_{\mathrm{m}} \le \frac{h}{2}, \tag{1}$$

where subscripts $\mathcal{P}_U$ and $\mathcal{P}_L$ are the material properties of the two constituents at the upper $(z = h/2)$ and lower $(z = -h/2)$ surfaces of the nanobeam, respectively, and k is a non–negative number (power law index), which controls the material variation profile through the thickness of the beam,where neutral surface reference can be evaluated by

$$\tilde{z} = \frac{\int_A z_{\mathrm{m}}\left[\lambda\left(z_{\mathrm{m}}\right) + 2\mu\left(z_m\right)\right]\mathrm{d}A}{\int_A \left[\lambda\left(z_{\mathrm{m}}\right) + 2\mu\left(z_m\right)\right]\mathrm{d}A}, \tilde{z} = z_{\mathrm{m}} - h_0. \tag{2}$$

Taking the physical neutral surface as a reference, the effective material properties take the following form:

$$\mathcal{P}(z) = \mathcal{P}_L + \left(\mathcal{P}_U - \mathcal{P}_L\right)\left(\frac{1}{2} + \frac{\tilde{z} + h_0}{h}\right)^k. \tag{3}$$

From this equation, it is seen that $\mathcal{P} = \mathcal{P}_L$, when $\tilde{z} = -\left(0.5h + h_0\right)$ and $\mathcal{P} = \mathcal{P}_U$ when $\tilde{z} = \left(0.5h - h_0\right)$. Young's modulus $(E(z))$, Poisson's ratio $(\nu(z))$, mass density $(\rho(z))$, microstructure material length scale $(l(z))$ of

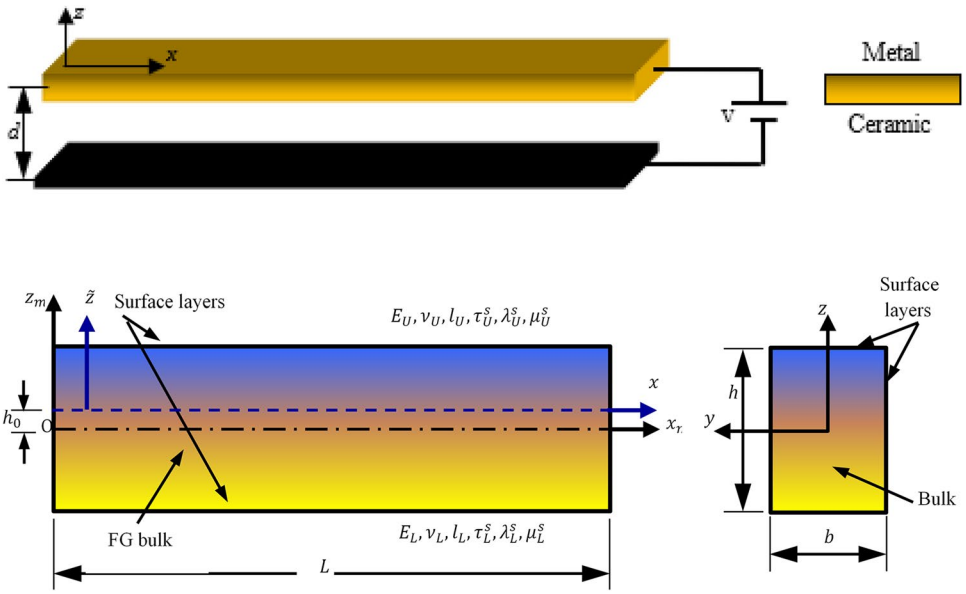

Fig. 1 Schematic of an FGM nanobeam subjected to an electrostatic force

the bulk, surface Lamé constants ($\lambda^s(z)$ and $\mu^s(z)$), surface residual stress ($\tau^s(z)$), and surface mass density ($\rho^s(z)$) can be expressed by power law gradation function, Eq. (3).

The displacement field based on the Euler–Bernoulli beam theory is expressed as

$$u_x(x,z,t) = u(x,t) - \tilde{z}w'(x,t), u_y(x,z,t) = 0, u_z(x,z,t) = w(x,t), \tag{4}$$

where u and w are the axial and lateral displacements of any point (x, z) on the mid-plane and t denotes time.

Based on Euler–Bernoulli beam theory in conjunction with the modified couple stress theory (MCST) presented by Yang et al. [78], the non-zero components of the infinitesimal strain vector (ε_{ij}), rotation vector (θ_i), and the symmetric curvature tensor (χ_{ij}), respectively, can be obtained as [5, 9, 66]

$$\varepsilon_{xx} = u' - \tilde{z}w'', \tag{5}$$

$$\theta_y = -w', \tag{6}$$

$$\chi_{xy} = \chi_{yx} = -\frac{1}{2}w'', \tag{7}$$

where the prime dash refers to the derivative with respect to the coordinate x and dot represents to the derivative with respect to the time t. Assuming a linear elastic behavior of the nanobeam, the bulk constitutive equations of the FG nanobeam can be expressed in terms of displacements as follows [5]:

$$\begin{Bmatrix} \sigma_{xx} \\ \sigma_{yy} = \sigma_{zz} \end{Bmatrix} = \begin{Bmatrix} [\lambda(z) + 2\mu(z)](u' - \tilde{z}w'') \\ \lambda(z)(u' - \tilde{z}w'') \end{Bmatrix}, \tag{8}$$

$$m_{xy} = m_{yx} = -\mu(z)l^2(z)w'', \tag{9}$$

where the other components are zero. σ_{ij} and m_{ij} are the force-stress component and the deviatoric part of the symmetric couple stress tensor, respectively. $\mu(z)$ and $\lambda(z)$ are the Lamé constants in classical elasticity, $l(z)$ refers to the material length scale parameter which is spatially dependent according to Eq. (3), and δ_{ij} denotes the Kronecker delta.

The surface energy effects are incorporated into the developed size-dependent model based on Gurtin–Murdoch surface elasticity theory [32], in which the surface constitutive relations of the FG micro/nanoscale beam can be formulated as, [3, 5]

$$\begin{Bmatrix} \tau_{xx}^{s\pm} \\ \tau_{nx}^{s\pm} \end{Bmatrix} = \begin{Bmatrix} \tau_s^{\pm} + E_s^{\pm}(u' - \tilde{z}w'') \\ \tau_s^{\pm}u_{n,x} = \tau_s^{\pm}n_z w' \end{Bmatrix}, \tag{10}$$

where $E_s^{\pm}$ is the surface elastic modulus, i.e. $E_s^{\pm} = \lambda_s^{\pm} + 2\mu_s^{\pm}$, where $\lambda_s^{\pm}$and $\mu_s^{\pm}$ are the surface Lamé constants, $\tau_s^{\pm}$ is the surface residual stress, and n_z represents the z-component of the outward unit normal $\boldsymbol{n}$ to the beam lateral surface. Here, the indices "+" and "−" represent the upper and lower surfaces of the nanobeam, respectively. The stresses of the surface layers must satisfy the equilibrium equations of Gurtin–Murdoch model; thus the normal component of the Cauchy stress σ_{xx} (Eq. (8)) is modified into [3, 5, 41]:

$$\sigma_{xx} = [\lambda(z) + 2\mu(z)](u' - \tilde{z}w'') + \frac{\nu(z)}{1-\nu(z)}\left[\left(\frac{1}{2}\Delta\tau_s + f(z)\overline{\tau}_s\right)w''\right], \tag{11}$$

in which $f(z) = -\left[2\left(\frac{z}{h}\right)^3 - \frac{3z}{2h}\right]$, $\overline{\tau}_s = \tau_s^+ + \tau_s^-$ and $\Delta\tau_s = \tau_s^+ - \tau_s^-$.

Hamilton's principle is employed to derive the governing equations and corresponding boundary conditions for the static analysis of FG nanobeams as following:

$$\int_{t_1}^{t_2} \left(\delta\mathcal{U} + \left[\delta \mathrm{W}_\mathrm{q} + \delta \mathrm{W}_\mathrm{s} + \delta \mathrm{W}_\mathrm{r}\right]\right)\mathrm{d}t \tag{12}$$

The first variation of the total strain energy of FG nanobeam can be obtained as follows:

$$\begin{aligned}\delta\mathcal{U} &= \frac{1}{2}\delta\int_0^L\int_A (\sigma_{ij}\varepsilon_{ij} + m_{ij}\chi_{ij})\mathrm{d}A\mathrm{d}x + \frac{1}{2}\delta\int_0^L\oint_{\partial A}\tau^s_{ij}\varepsilon_{ij}\mathrm{d}S\mathrm{d}x\\ &= \frac{1}{2}\delta\int_0^L\left\{\int_A (\sigma_{xx}\varepsilon_{xx} + 2m_{xy}\chi_{xy})\mathrm{d}A + \oint_{\partial A}(\tau^\mathrm{s}_{xx}\varepsilon_{xx} + 2\tau^\mathrm{s}_{nx}\varepsilon_{nx})\mathrm{d}S\right\}\mathrm{d}x\end{aligned} \tag{13}$$

in which $\varepsilon_{nx} = 0.5w'n_z$. Substituting Eqs. (5, 7, 9, 10), Eq. (13) can be obtained in terms of the stress resultants as follows:

$$\begin{aligned}\delta\mathcal{U} = \int_L \Big\{ &\left[N_{xx} + N^\mathrm{s}_{xx} + \frac{1}{2}\mathcal{T}_{11}w'' - \frac{1}{2}\mathcal{C}_{P1}\right]\delta u'\\ &-\left[M_{xx} + Y_{xy} + M^\mathrm{s}_{xx} - \frac{1}{2}\mathcal{P}_{A1} - \frac{1}{2}\mathcal{T}_{11}u'\right]\delta w''\\ &+\left[\mathcal{S}_P w'\right]\delta w'\Big\}\mathrm{d}x,\end{aligned} \tag{14}$$

where the forces and moments resultants are expressed as

$$\begin{Bmatrix} N_{xx} \\ M_{xx}\end{Bmatrix} \equiv \int_A \begin{Bmatrix}1\\ \tilde{z}\end{Bmatrix}\sigma_{xx}\mathrm{d}A = \begin{Bmatrix}A_{xx}\\ B_{xx}\end{Bmatrix}u' - \begin{Bmatrix}B_{xx} - \mathcal{T}_{11}\\ D_{xx} - \mathcal{T}_{22}\end{Bmatrix}w'', \tag{15a}$$

$$\begin{Bmatrix} N^\mathrm{s}_{xx} \\ M^\mathrm{s}_{xx}\end{Bmatrix} \equiv \oint_{\partial A} \begin{Bmatrix}1\\ \tilde{z}\end{Bmatrix}\tau^s_{xx}\mathrm{d}S = \begin{Bmatrix}\mathcal{C}_{P1}\\ \mathcal{P}_{A1}\end{Bmatrix} + \begin{Bmatrix}\mathcal{C}_{P2}\\ \mathcal{P}_{A2}\end{Bmatrix}u' - \begin{Bmatrix}\mathcal{P}_{A2}\\ I_P\end{Bmatrix}w'', \tag{15b}$$

$$Y_{xy} \equiv \int_A m_{xy}\mathrm{d}A = -S_{xy}w'', \tag{15c}$$

in which,

$$\left\{A_{xx}\ B_{xx}\ D_{xx}\right\} = \int_A \overline{E}(z)\left\{1\ \tilde{z}\ \tilde{z}^2\right\}\mathrm{d}A, \overline{E}(z) = \frac{E(z)}{\left(1-\nu(z)^2\right)}\ \text{if}\ b \geq 5h\ \text{else}\ \ \overline{E}(z) = E(z), \tag{16a}$$

$$S_{xy} = \int_A \mu(z)l(z)^2\mathrm{d}A, \mu(z) = \frac{E(z)}{2(1+\nu(z))}, \tag{16b}$$

$$\left\{\mathcal{C}_{P1}\ \mathcal{P}_{A1}\ \mathcal{S}_P\right\} = \oint_{\partial A}\tau_s(z)\left\{1\ \tilde{z}\ n_z^2\right\}\mathrm{d}S, \tag{16c}$$

$$\left\{\mathcal{C}_{P2}\ \mathcal{P}_{A2}\ I_P\right\} = \oint_{\partial A} E_\mathrm{s}(z)\left\{1\ \tilde{z}\ \tilde{z}^2\right\}\mathrm{d}S, \tag{1d}$$

$$\left\{\mathcal{T}_{11}\ \mathcal{T}_{22}\right\} = \int_A f_\tau\left\{1\ \tilde{z}\right\}\mathrm{d}A, f_\tau = \frac{\nu(z)}{1-\nu(z)}\left[\left(\frac{1}{2}\Delta\tau_\mathrm{s} + f(z)\overline{\tau}_s\right)\right]. \tag{16e}$$

The virtual work done by the electrostatic and intermolecular forces ($\delta \mathrm{W}_\mathrm{q}$) is

$$\delta \mathrm{W}_\mathrm{q} = \int_0^L \left[q_\mathrm{e} + q_\mathrm{vdW} + q_\mathrm{C}\right]\delta w\mathrm{d}x. \tag{17}$$

The electrostatic force q_e per unit length of the nanobeam including the first-order fringing field correction can be defined as [53, 52, 69]

$$q_\mathrm{e} = \frac{\varepsilon_0 b v^2}{2[d-w]^2} + \frac{0.65\varepsilon_0 v^2}{2[d-w]}, \tag{18}$$

in which, $\varepsilon_0 = 8.854\times10^{-12}\mathrm{C}^2\mathrm{N}^{-1}\mathrm{m}^{-2}$ denotes the vacuum permittivity, v is the voltage applied on the system, and d represents the initial distance between the nanobridge and fixed substrate. When the width of the nanobeam is much larger than the gap between beam and substrate (i.e. $b \gg d$), the effect of fringing field can be neglected. For nanobeams with the width in order of the initial gap, effect of fringing field is important and neglecting this phenomenon underestimates the electrostatic load and overestimates the pull-in voltage of the nanobeam, Rahaeifard et al. [51]. Regarding the interatomic forces q_int, two interaction regimes can be considered; the first one belongs to the small separation sizes (typically below several tens of nanometers, Soroush et al. [69] and [1] that vdW force (q_vdW) dominates. The second one accomplished with the large separation sizes (typically above several tens of nanometers, Soroush et al. [69] and Abdi et al. [1] that Casimir force (q_Cas) dominates. These interatomic forces per unit length of the nanobeam are given by

$$q_\mathrm{vdW} = \frac{\mathrm{A_H}b}{6\pi(d-w)^3}\ \text{and}\ q_\mathrm{Cas} = \frac{b\pi^2 h_\mathrm{P}\overline{C}}{240(d-w)^4}, \tag{19}$$

where $\mathrm{A_H} = (0.4\text{upto}4)\times10^{-19}\mathrm{J}$ is the Hamaker constant, $h_\mathrm{P} = 1.055\times10^{-34}\mathrm{Js}$ denotes the reduced Planck's constant divided by 2π, and $\overline{C} = 2.998\times10^8\mathrm{m/s}$ is the light speed.

In the case of FG nanobeams with immovable boundary conditions, the virtual work due to midplane stretching of the nanobeam (δW_s) and residual stress (δW_r) is, respectively, given by

$$\delta W_s = \delta\left(-N_r \int_0^L w'^2 dx\right), \tag{20}$$

$$\delta W_r = -\frac{1}{8} K_a \delta\left(\int_0^L w'^2 dx\right)^2, K_a = \int_A \frac{\overline{E}(z)}{L} dA \tag{21}$$

where the axial force $N_r = s_r bh$, in which the effective residual stress $s_r = (1-\nu)s_0$; otherwise, $s_r = s_0$ for narrow beams ($b < 5\,h$), where s_0 is the initial biaxial residual stress in the beam, Rokni et al. [55]. For the case of cantilever nanobeams, δW_s and δW_s are set to zero. Substituting Eqs. (14), (17), (20), and (21) into Eq. (13), and integrating by parts, results in the following size-dependent nonlinear governing equations of motion in terms of displacements,

$$\delta u : \left(A_{xx} + \mathcal{C}_{P2}\right)u'' - \left(\mathcal{B} + \frac{1}{2}\mathcal{T}_{11}\right)w''' = 0, \tag{22a}$$

$$\delta w : -\mathcal{D}w'''' + \left(\mathcal{B} + \frac{1}{2}\mathcal{T}_{11}\right)u''' + \left[\mathcal{S}_P + N_r + \frac{1}{2}K_a\left(\int_0^L w'^2 dx\right)\right]w'' + q_e + q_{vdW} + q_{Cas} = 0, \tag{22b}$$

subject to the following boundary conditions at $x = 0$ and $x = L$.

$$\text{Either } u = \tilde{u} \text{ or } \left(A_{xx} + \mathcal{C}_{P2}\right)u' - \left(\mathcal{B} + \frac{1}{2}\mathcal{T}_{11}\right)w'' + \frac{1}{2}\mathcal{C}_{P1} = 0, \tag{23a}$$

$$\text{Either } w = \tilde{w} \text{ or } \mathcal{D}w''' - \left(\mathcal{B} + \frac{1}{2}\mathcal{T}_{11}\right)u'' - \left(\mathcal{S}_P + N_r + \frac{1}{2}K_a\int_0^L w'^2 dx\right)w' = 0, \tag{23b}$$

$$\text{Either } w' = \tilde{w}' \text{ or } \left(\mathcal{B} + \frac{1}{2}\mathcal{T}_{11}\right)u' - \mathcal{D}w'' + \frac{1}{2}\mathcal{P}_{A1} = 0, \tag{23c}$$

where

$$\mathcal{D} = D_{xx} - \mathcal{T}_{22} + S_{xy} + I_P \text{ and } \mathcal{B} = B_{xx} - \mathcal{T}_{11} + \mathcal{P}_{A2}.$$

Substitution of Eq. (22a) into Eq. (22b) yields Eq. (22b) in terms of the transverse displacement only as follows:

$$\left[\mathcal{D} - \frac{1}{A_{xx} + \mathcal{C}_{P2}}\left(\mathcal{B} + \frac{1}{2}\mathcal{T}_{11}\right)^2\right]w'''' - \left[\mathcal{S}_P + N_r + \frac{1}{2}K_a\left(\int_0^L w'^2 dx\right)\right]w'' = q_e + q_{vdW} + q_{Cas}. \tag{24}$$

For convenience, introducing the nondimensional variables $\hat{x} = x/L$ and $\hat{w} = w/d$ in Eq. (24), multiplying the result by $L^4/E_L Id$ and dropping the hats, we obtain the following nondimensional governing equation:

$$\overline{\mathbb{D}}w'''' - \left[\overline{\mathcal{S}}_P + \overline{N}_r + \overline{K}_a\left(\int_0^1 w'^2 dx\right)\right]w'' = V^2\left[\frac{1}{(1-w)^2} + \frac{c_f}{(1-w)}\right] + \frac{c_{vdW}}{(1-w)^3} + \frac{c_{Cas}}{(1-w)^4}. \tag{25}$$

Further, the nondimensional boundary conditions are obtained as

$$\text{Clamped (C)} : w = 0 \text{and} w' = 0, \tag{26a}$$

$$\text{Simply supported (S)} : w = 0 \text{and} -\overline{\mathcal{D}}w'' + \overline{\mathcal{P}}_{A1} = 0, \tag{26b}$$

$$\text{Free (F)} : -\overline{\mathbb{D}}w''' + \left(\overline{\mathcal{S}}_{P1} + \overline{N}_r + \overline{K}_a\int_0^1 w'^2 dx\right)w' = 0 \text{and} -\overline{\mathbb{D}}w'' + \overline{\mathbb{K}} = 0. \tag{26c}$$

The dimensionless coefficients appear in Eqs. (25) and (26a–26c) and are defined as

$$\begin{cases} \mathbb{D} = \mathcal{D} - \frac{1}{A_{xx}+\mathcal{C}_{P2}}\left(\mathcal{B} + \frac{1}{2}\mathcal{T}_{11}\right)^2 \\ \mathbb{K} = \frac{1}{2}\left[\mathcal{P}_{A1} - \frac{\mathcal{C}_{P1}}{A_{xx}+\mathcal{C}_{P2}}\left(\mathcal{B} + \frac{1}{2}\mathcal{T}_{11}\right)\right] \\ \left\{ V \;\; c_f \;\; c_{vdW} \;\; c_{Cas} \right\} = \left\{ \sqrt{\frac{\epsilon_0 bL^4}{2E_L Id^3}}\mathrm{v} \;\; \frac{0.65d}{b} \;\; \frac{bL^4 A_H}{6\pi E_L Id^4} \;\; \frac{\pi^2 bL^4 h_P \bar{c}}{240 E_L Id^5} \right\} \\ \left\{ \overline{\mathcal{D}} \;\; \overline{\mathbb{D}} \;\; \overline{\mathbb{K}} \;\; \overline{N}_r \;\; \overline{K}_a \;\; \overline{\mathcal{S}}_P \;\; \overline{\mathcal{P}}_{A1} \right\} = \frac{1}{E_L I}\left\{ \mathcal{D} \;\; \mathbb{D} \;\; \frac{E_L I}{d}\mathbb{K} \;\; L^2 N_r \;\; \frac{Ld^2}{2}K_a \;\; L^2\mathcal{S}_P \;\; L^2\overline{\mathcal{P}}_{A1} \right\} \end{cases}. \tag{27}$$

3 Analytical approach

3.1 Pull-in closed form

To derive a closed-form solution to Eqs. (25, 26a–26c), the normalized displacement of the FG micro/nanobeam $w(x)$ is approximated as

$$w(x) \cong u\varphi(x), \tag{28}$$

where $\varphi(x)$ is deflection shape function satisfying the boundary conditions and u denotes a scaling of the displacement function such that Eq. (25) is satisfied. Note that $\varphi(x)$ is normalized such that $\max(|\varphi(x)|) = 1$ and hence u describes the mid-point and tip deflections of, respectively, clamped–clamped and clamped-free FG nanobeams.

The deflection shape function $\varphi(x)$ is given in Table 1 for fully clamped and clamped-free nanobeams.

Substitution of Eq. (28) into Eq. (25) and multiplying the result by $\varphi(x)$, then integrating with respect to x between 0,1 yields

$$\begin{aligned}\left(i_{04}\overline{\mathbb{D}} - i_{02}\left(\overline{\mathcal{S}}_{\mathrm{P}} + \overline{N}_{\mathrm{r}}\right)\right)u - i_{02}i_{11}\overline{K}_a u^3 = V^2 \int_0^1 \left[\frac{1}{(1-u\varphi(x))^2} + \frac{c_f}{(1-u\varphi(x))}\right]\varphi(x)\mathrm{d}x \\ + \int_0^1 \left[\frac{c_{\mathrm{vdW}}}{(1-u\varphi(x))^3} + \frac{c_{\mathrm{Cas}}}{(1-u\varphi(x))^4}\right]\varphi(x)\mathrm{d}x,\end{aligned} \tag{29}$$

where

$$\left\{ i_{02} \;\; i_{04} \;\; i_{11} \right\} = \int_0^1 \left\{ \varphi\varphi'' \;\; \varphi\varphi'''' \;\; \varphi'^2 \right\}\mathrm{d}x. \tag{30}$$

In this study, the integral forms of the electrostatic and intermolecular forces in the right-hand side of Eq. (29) are approximated in the form of algebraic functions of u as follows:

$$\int_0^1 \left[\frac{1}{(1-u\varphi(x))^2} + \frac{c_{\mathrm{f}}}{(1-u\varphi(x))}\right]\varphi(x)\mathrm{d}x \cong \frac{a_0}{\left(1-a_1u\right)^{a_2}}, \tag{31}$$

$$\int_0^1 \frac{\varphi(x)}{(1-u\varphi(x))^3}\mathrm{d}x \cong b_3u^3 + b_2u^2 + b_1u + b_0, \tag{32a}$$

$$\int_0^1 \frac{\varphi(x)}{(1-u\varphi(x))^4}\mathrm{d}x \cong c_3u^3 + c_2u^2 + c_1u + c_0. \tag{32b}$$

At specific values of u in the range $0 \le u \le 0.5$, the values of the integrals in the left-hand sides of Eqs. (31, 32a, 32b) can be accurately computed. Then, the least squares method is applied to determine the coefficients in the right-hand sides of Eqs. (32a, 32b). However, such classical method is not applicable for Eq. (31).

Particle Swarm Optimization (PSO) is a powerful evolutionary technique for many optimization applications due to its high performance and flexibility. PSO was first developed by Kennedy and Eberhart [35]. PSO shares many similarities with evolutionary computation techniques such as Genetic Algorithms (GA). In PSO, the process is initialized with a population of random solutions and continuing searching for optima by updating generations. However, unlike GA, PSO has no evolution operators, such as mutation and crossover. PSO has been successfully applied in many research and application areas, Eberhart et al. [19]. It is demonstrated that, compared with other methods, PSO gets better results in a faster and cheaper way. Therefore, in the present study, a PSO algorithm is used to approximate the coefficients in the right-hand side of Eq. (31). For this equation, the coefficients are determined to minimize an objective function defined as the sum of squares of the difference of the two sides at the chosen values of u.

Substitution of Eqs. (31, 32a, 32b) in Eq. (29), reduces to

$$A_1u + A_3u^3 = V^2\frac{a_0}{\left(1-a_1u\right)^{a_2}} + \left(k_3u^3 + k_2u^2 + k_1u + k_0\right), \tag{33}$$

where

$$\left\{ A_1 \;\; A_3 \right\} = \left\{ i_{04}\overline{\mathbb{D}} - i_{02}\left(\overline{\mathcal{S}}_{\mathrm{P}} + \overline{N}_r\right) \;\; -i_{02}i_{11}\overline{K}_a \right\}, \tag{34}$$

$$k_i = \begin{cases} c_{\mathrm{vdW}}b_i & \text{for vdW force} \\ c_{\mathrm{Cas}}c_i & \text{for Casimir force} \end{cases}, i = 0, 1, 2, 3. \tag{35}$$

Notice that the coefficients in the left-hand side of Eq. (33) are dependent on mechanical parameters $\overline{\mathbb{D}}, \overline{\mathcal{S}}_{\mathrm{P}}, \overline{N}_{\mathrm{r}}$, and $\overline{K}_{\mathrm{a}}$. In the right-hand side, the first term corresponds to the electrostatic force including fringing field, while the last term corresponds to the intermolecular forces.

Equation (33) represents an implicit algebraic equation of the deflection amplitude u and applied voltage V. Differentiating Eq. (33) with respect to u yields

$$A_1 + 3A_3u^2 = V^2\frac{a_0}{\left(1-a_1u\right)^{a_2}}\frac{a_1a_2}{\left(1-a_1u\right)} + 2V\frac{\mathrm{d}V}{\mathrm{d}u}\frac{a_0}{\left(1-a_1u\right)^{a_2}} + \left(3k_3u^2+2k_2u+k_1\right). \tag{36}$$

Multiplying Eq. (36) by $\left(1-a_1u\right)$ and subtracting the result from Eq. (33) and since the mathematical condition of pull-in phenomena is $\mathrm{d}V/\mathrm{d}u = 0$, the pull-in deflection u_{pi} must satisfy the following relation:

$$C_0u_{\mathrm{pi}}^3 + C_1u_{\mathrm{pi}}^2 + C_2u_{\mathrm{pi}} + C_3 = 0 \tag{37}$$

where

$$\begin{Bmatrix} C_0\\ C_1\\ C_2\\ C_3 \end{Bmatrix} = \begin{Bmatrix} a_1\left(3+a_2\right)A_3 - a_1k_3\left(a_2+3\right)\\ -3A_3 - \left(a_1a_2k_2 - 3k_3 + 2k_2a_1\right)\\ a_1\left(a_2+1\right)A_1 - \left(k_1a_1 + a_2a_1k_1 - 2k_2\right)\\ -A_1 - \left(a_1a_2k_0 - k_1\right) \end{Bmatrix}. \tag{38}$$

Equation (37) is a cubic algebraic equation in the pull-in deflectionu_{pi}. Once u_{pi} is obtained, the pull-in voltage V_{pi} is computed from Eq. (33). The integration parameters i_{02}, i_{11} and i_{04} defined in Eq. (30) as well as the used shape functions $\varphi(x)$ are reported in Table 1 for the C–C and C–F nanobeams. On the other hand, the approximation parameters (a_0, a_1, a_2 in Eq. (31)) are dependent on c_{f} and are computed using PSO. Table 2 reports these parameters at some values of c_{f}. The case of $c_{\mathrm{f}} = 0$ corresponds to $b \gg d$, where the fringing field effect is neglected.

3.2 Freestanding closed form

When considering a nanosystem, it is worth noting that one of the most important parameters is its freestanding behavior. In the absence of electrostatic force (applied voltage), interatomic Casimir and van der Waals forces may tend the nanobeam to undergo a primary displacement, i.e. the movable electrode falls on the fixed electrode, and thus the nanobeam may behave unstably. Such effect can induce undesired adhesion in freestanding during the fabrication and operation procedures of such systems, which should be considered when either the gap distance between the movable electrode and the field one is small or the length of the nanobeam is greater than a certain magnitude, Farrokhabadi et al. [26]. In this regard, modeling of intermolecular interatomic Casimir and van der Waals force-induced instability is crucial for investigating the performance of nanoactuators made of FGMs.

When the nanoactuator becomes freestanding, the voltage difference between the nanobeam and the substrate vanishes. Accordingly, the smallest amount of intermolecular force that causes the movable electrode to fall on the fixed electrode in the absence of electrostatic force is called critical intermolecular force. Behavior of a freestanding nanoactuator is a special case of the present study. Setting the applied voltage $V = 0$ in Eqs. (33) yields

$$c_{\mathrm{vdW}} = \frac{A_1u + A_3u^3}{b_3u^3 + b_2u^2 + b_1u + b_0}, \tag{39}$$

$$c_{\mathrm{Cas}} = \frac{A_1u + A_3u^3}{c_3u^3 + c_2u^2 + c_1u + c_0}, \tag{40}$$

where A_1, A_3 are defined by Eq. (34) and coefficients b_i, c_i, $i = 0, 1, 2, 3$ are given in Table 3 for C–C and C–F nanobeams.

Let the critical parameters of Eqs. (39, 40) be, respectively $(u^*_{\mathrm{vdW}}, c^*_{\mathrm{vdW}})$ and $(u^*_{\mathrm{Cas}}, c^*_{\mathrm{Cas}})$. Once the critical intermolecular parameters c^*_{vdW} and c^*_{Cas} are determined, the definitions of c_{vdW} and c_{Cas} in Eq. (27) can be used to compute the permissible maximum length (called the detachment length) and minimum initial gap and of the of freestanding nanobeams as follows:

$$\text{The detachment length}: L^*_{\mathrm{Cas}} = d^{5/4}\sqrt[4]{\frac{20E_1h^3}{\pi^2h_P\bar{c}}c^*_{\mathrm{Cas}}}$$
$$\text{and } L^*_{\mathrm{vdW}} = d\sqrt[4]{\frac{\pi E_1h^3}{2\mathrm{A}_H}c^*_{\mathrm{vdW}}}, \tag{41}$$

Table 1 Trial shape function $\varphi(x)$ for the clamped–clamped and clamped-free FG nanobeams and associated integrals (Eq. (30))

Beam type	Trial shape function $\varphi(x)$	Integration parameters
C–C	$\varphi(x) = \frac{1}{1.58815}\left[\cosh(mx) - \cos(mx) - \frac{\cosh(m)-\cos(m)}{\sinh(m)-\sin(m)}(\sinh(mx) - \sin(mx))\right]$, $m = 4.73004074$	$i_{02} = -4.877693688$ $i_{04} = 198.4615997$ $i_{11} = 4.877693672$
C-F	$\varphi(x) = \frac{1}{2}\left[\cosh(mx) - \cos(mx) - \frac{\sinh(m)-\sin(m)}{\cosh(m)+\cos(m)}(\sinh(mx) - \sin(mx))\right]$, $m = 1.875104069$	$i_{02} = 0.2145609034$ $i_{04} = 3.090590853$ $i_{11} = 1.161944579$

$$\text{Minimum gap}: d^*_{\text{Cas}} = L^{4/5}\sqrt[5]{\frac{\pi^2 h_P \bar{c}}{20E_1 h^3 c^*_{\text{Cas}}}}$$
$$\text{and } d^*_{\text{vdW}} = L\sqrt[4]{\frac{2\text{A}_H}{\pi E_1 h^3 c^*_{\text{vdW}}}}. \quad (42)$$

4 Model validation

4.1 Proposed approximation in Eqs. (31, 32a, 32b)

As mentioned in Sect. 3, the basic idea to get the proposed closed-form approximations is to replace the integral forms representing electrostatic, fringing, and intermolecular forces in Eq. (29) by non-integral algebraic functions. For the purpose of validation of these approximations introduced in Eqs. (31, 32a, 32b), the integral and non-integral forms are computed at different values of the maximum deflection, u, as presented in Figs. 2 and 3 for the C–C and C–F cases. Figure 2 shows the accuracy of the PSO approximation given in Eq. (31) for the terms of electrostatic and fringing (with $d/b = 1$) forces, while Fig. 3 corresponds to Eqs. (32a, 32b) that associates with approximations of van der Waals and Casimir forces. The maximum relative errors E_{r}^{∞} are reported in Table 4 for the proposed approximations, where the error is the difference between the exact integral values and the corresponding algebraic functions in Eqs. (31, 32a, 32b).

4.2 Validation of pull-in voltage

To validate the present analytical closed-form approach for predicting the static pull-in phenomenon, the static pull-in voltage of microcantilevers with different geometric and material properties are obtained and compared with some available analytical and numerical results in Table 5. For clamped–clamped nanobeams with different geometric, material properties and axial residual stresses, the static pull-in voltages obtained using the proposed closed-form are compared with similar ones available in literature in Table 6. Based on the results of Tables 5 and 6, the accuracy of present analytical closed-form approach can be observed. It should be noted that for comparison in the above validations, the nanobeams are assumed homogeneous, i.e. $k = 0$, and are modeled based on the classical elasticity theory (CT), i.e. all the nonclassical surface and microstructure parameters are set to zero. Also, the effects of fringing field and intermolecular van der Waals and Casimir forces are neglected.

To validate the present closed-form model in the presence of microstructure effect, homogeneous cantilever microactuators are considered and modeled based on the modified couple stress theory (MCST), i.e. all the surface parameters are set to zero. For the aim of comparison, the influences of fringing field and intermolecular forces are neglected in this validation. The geometrical and material parameters used in Rahaeifard et al. [51] and Rokni et al. [55] are E =169.2 GPa, ν=0.239, b=50 μm, h=2.94 μm, and d=1.05 μm. The obtained results of the static pull-in voltage for different beam lengths and microstructure material length scale parameters are displayed in Table 7 and compared with corresponding values reported in Rokni et al. [55] based on a closed-form solution and Rahaeifard et al. [51] where a numerical approach was used.

Next, the proposed closed-form solution is validated by investigating the pull-in characteristics of a micro/nanocantilever including the effects of fringing field and intermolecular forces. The obtained results are compared with Radi et al. [49], who modeled a micro/nanocantilever actuated by electrostatic force including fringing field and subject to Casimir or van der Waals forces based on the classical continuum mechanics (CL). Rather than determining the pull-in parameters, they estimated lower and upper bounds of the parameters, namely the pull-in voltage parameter (β_l and β_u) and the normalized tip displacement (u_l and u_u). For comparison with Radi et al. [49], Eq. (25) is reduced to account for a classical cantilever nanobeam by setting

Table 2 Coefficients of approximation (a_0, a_1, a_2) in Eq. (31) for various fringing field parameters c_{f}

	$c_{\text{f}} = 0.65(d/b)$	a_0	a_1	a_2
C–C	0.0	0.523127954802096	0.997496563158028	1.519042711142470
	0.65 × 1/50	0.530337989567136	1.008794228934500	1.487159569030100
	0.65 × 1/10	0.557320816780667	1.012407974951880	1.450408267732250
	0.65 × 1/2	0.693456113366252	1.048974660627200	1.267460739469660
	0.65	0.862852855161830	1.056886076090580	1.157757467970810
C–F	0.0	0.391581895921048	0.956563131373158	1.331439465244600
	0.65 × 1/50	0.396275296263726	0.948106024063029	1.341945603173360
	0.65 × 1/10	0.417631602595171	0.983617243441750	0.983617243441750
	0.65 × 1/2	0.519080342333035	0.998800736182284	1.117609064675130
	0.65	0.645855527683283	1.005190511721540	1.021182912266340

Table 3 Coefficients of approximation in Eqs. (32a, 32b): approximation of $\int_0^1 \frac{1}{(1-u\varphi)^r}\varphi \mathrm{d}x$

	van der Waals force ($r=3$), Eq. (32a)				Casimir force ($r=4$), Eq. (32b)			
	b_3	b_2	b_1	b_0	c_3	c_2	c_1	c_0
C–C	17.9699071753	− 4.5374333346	1.9651785203	0.5101494421	51.2226530837	− 17.1257097294	4.0648401872	0.4808110277
C–F	7.6970124549	− 1.5409055297	1.0616078391	0.3863159541	21.2764246197	− 6.2491912389	1.9713552500	0.3750585890

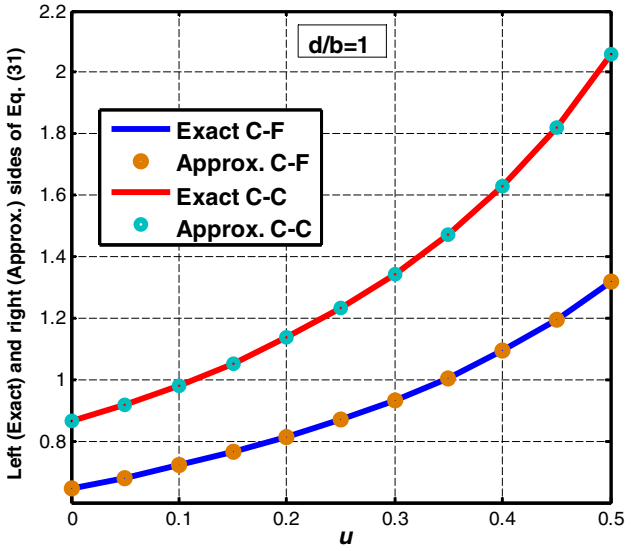

Fig. 2 Exact and PSO approximation of the integral function in Eq. (31)

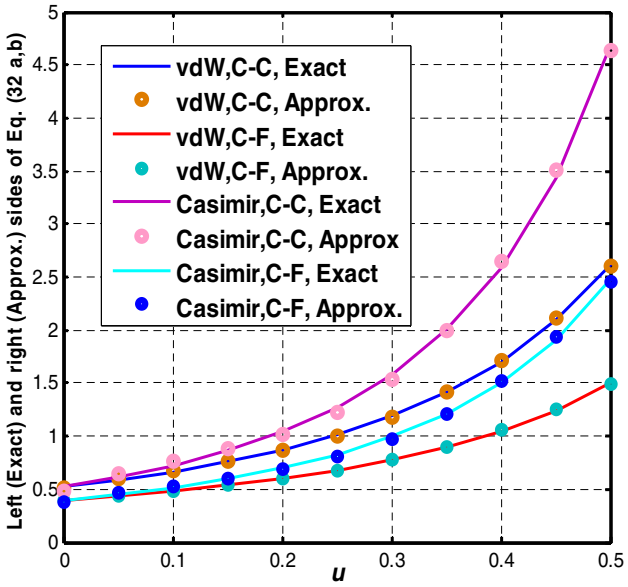

Fig. 3 Exact and pproximation of the integral function in Eqs. (32a, 32b)

$\overline{S}_{\mathrm{P}} = \overline{N}_{\mathrm{r}} = \overline{K}_{\mathrm{a}} = 0, \overline{\mathbb{D}} = 1$, and defining the pull-in voltage parameter $\beta = V^2$; thus the governing equation becomes

$$\frac{\mathrm{d}^4 w}{\mathrm{d}x^4} = \beta\left[\frac{1}{(1-w)^2} + \frac{c_{\mathrm{f}}}{(1-w)}\right] + \frac{c_{\mathrm{vdW}}}{(1-w)^3} + \frac{c_{\mathrm{Cas}}}{(1-w)^4}. \tag{43}$$

Results are reported in Table 8 for some specific values of the initial gap-to-width ratio d/b, which controls the fringing field effects and for various values of the coefficients c_{vdW} and c_{Cas}. In this table, the normalized pull-in tip displacement and pull-in voltage are displayed, respectively, as u and β, determined by the present closed-form approach and by lower and upper bounds (u_l, u_u) and (β_l, β_u) reported in Radi et al. [49]. It is noticed that excellent agreement is observed, since almost of the parameter values computed by the present closed-form PSO-based approach lie within the lower and upper bounds computed in Radi et al. [49]. Note that negative values of $\beta = V^2$ appearing in Table 8 imply sudden occurrence of the pull-in instability as no real solution can be obtained for the tip displacement and that at these situations the intermolecular forces exceed their critical values.

Table 4 Maximum relative error E_r^{∞} in the proposed PSO approximation given in Eqs. (31, 32a, 32b)

Beam type	Equation (31), $d/b = 1$	Equation (32a)	Equation (32b)
C–C	0.000424	0.043	0.070
C–F	0.000174	0.017	0.026

4.3 Validation of freestanding behavior

To determine the critical points of the intermolecular parameters c_{vdW} and c_{Cas} based on Eqs. (39) and (40), respectively, they are plotted in Fig. 4 based on the classical elasticity theory for a cantilever nanobeam. For the purpose of comparison with Duan et al. [18], the material is assumed to be homogeneous, $k = 0$. The critical points on the curves of Eqs. (39 and 40) are, respectively, $(u^*_{\mathrm{vdW}}, c^*_{\mathrm{vdW}}) = (0.34, 1.204)$ and $(u^*_{\mathrm{Cas}}, c^*_{\mathrm{Cas}}) = (0.27, 0.9372)$ as displayed in the

Table 5 Comparison of static pull-in voltage of homogeneous microcantilevers obtained from the present closed-form method with data from the literature based on the classical analysis ($E = 169$ GPa, $\nu = 0.06$)

Geometric dimensions (μm)s				Static pull-in voltage (volt)							
L	b	h	d	Osterberg and Senturia [46]	Chowdhury et al. [16]	Haluzan et al. [33]	Rokni et al. [55]	Hu et al. [34]	Kuang and Chen [36]	Younis [81]	Present
20,000	5000	57	92	–	–	–	–	68.5	68.5	–	69.37
100	50	3	1	37.9	37.84	37.85	37.88	–	37.49	–	37.97
150	50	3	1	16.8	16.83	16.85	16.84	–	16.67	–	16.88
100	10	1	1	–	–	–	–	–	–	7.14	7.11

figure. Based on the classical elasticity theory (CT), Duan et al. [18] reported that for a homogeneous cantilever $u^*_{\text{Cas}} = 0.269401$ and $c^*_{\text{Cas}} = 0.932616$, which agree well with the corresponding values displayed in Fig. 4. Also, Radi et al. [49] have reported lower and upper bounds for c^*_{vdW} as [1.1967, 1.2171], u^*_{vdW} as [0.3350, 0.3423] and c^*_{Cas} as [0.9326, 0.9492], u^*_{Cas} as [0.2694, 0.2756], which agree well with the present predicted critical values.

5 Parametric studies

In this section, selected numerical results are presented to demonstrate the capability of the developed closed-form approach to investigate the influences of incorporating surface energy and microstructure theories on the pull-in instability and freestanding behavior of electrically actuated clamped–clamped (C–C) and clamped–free (C–F) FG nanobeams. To demonstrate the influence of couple stress and surface energy simultaneously together or individually, four various analyses are considered: (1) the classical theory (CT), based on the classical continuum mechanics theory, where all surface and microstructure parameters are set to zero: (2) analysis based on the modified couple stress theory only (MCST): (3) analysis based on surface elasticity theory only (SET), and (4) fully nonclassical analysis incorporating the simultaneous effects of surface energy and modified couple stress (CSSE). Also, effects of fringing field and the intermolecular Casimir and van der Waals forces are simultaneously included.

Throughout the following analyses, consider an FG beam possessing the material properties given in Table 9, assuming a material length scale parameter ratio $l_L/l_U = 1.5$. The geometrical parameters of the beam are $h = 3l_U$, $L = 40h$, $b = 5h$, and $d = 0.6h$; otherwise, other values of the material or geometrical parameters are defined. Further, Poisson's effect is included in this parametric study and $N_r = 0$. Due to the assumption in Eq. (28) that $w(x) \cong u\varphi(x)$, where $\varphi(x)$ is deflection shape function satisfying the classical boundary conditions, the proposed closed-form does not account for the nonclassical boundary conditions. In fact, nonclassical boundary conditions occur only at a free end due nonzero surface residual stress τ^s as can be seen from Eq. (26c) since $\overline{\mathcal{S}}_{\text{P1}} = \overline{\mathbb{K}} = 0$ if $\tau^s = 0$.

5.1 Effect of the material composition

To understand the effect of the material composition on the pull-in instability of the nanobeam, the distribution of bulk Young's modulus through thickness $E(z)$ for various values of the gradient index k is plotted in Fig. 5. Note first that at upper edge of the beam ($z = h/2$), the material is pure ceramic. As the value of k increases, the constitution of ceramic in the material decreases and results in lower Young's modulus distribution, i.e. as k tends to ∞, the material becomes pure metal. Since the beam stiffness depends mainly on Young's modulus, one can expect that increasing k would result in reducing the beam stiffness. However, incorporation of micro/nanoscale effects (couple stress and surface energy) adds important contributions to the stiffness of the beam as can be seen in the coefficients of the governing equation (Sect. 2).

First, the effect of the gradient index on the pull-in voltage of a nanobeam is investigated taking into consideration the influence of MCST. The variations of the pull-in voltage with the gradient index k are shown in Fig. 6a for a clamped–clamped nanobeam and in Fig. 6b for a cantilever nanobeam, according to CT and MCST with and without fringing field effect.

Some numerical values of the pull-in voltage at different gradient indices are provided in Table 10. From these results, one can conclude that increasing the gradient index decreases the pull-in voltage of the nanobeam. Compared with CT, MCST results in increasing the beam bending rigidity. Therefore, the microstructure size-dependent effect provides a hardening behavior that enhances the elastic resistance of the nanobeam and accordingly requires higher applied voltage before the instability occurs. Also, including fringing field acts as additional electrostatic force that increases the nanobeam deflection and results in lower

Table 6 Comparison of static pull-in voltage of homogeneous clamped–clamped nanobeams obtained from the present method with data from the literature based on the classical analysis

Material parameters		Geometric dimensions (μm)				Residual stress	Static pull-in voltage (volts)						
E (GPa)	ν	L	b	h	d	s_0(MPa)	Pamidighantam et al. [48]	Sadeghian et al. [56]	Kuang and Chen [36]	Tahan and Askari [70]	Tilmans and Legtenberg [72]	Rokni et al. [55]	Present
169	0.06	250	50	3	1	0	40.38	39.13	–	–	–	39.40	39.31
169	0.06	250	50	3	1	100	58.87	57.62	–	–	–	57.37	57.44
169	0.06	250	50	3	1	− 25	34.12	33.63	–	–	–	33.43	33.27
169	0.06	350	50	3	1	0	20.60	20.36	–	–	–	20.10	20.06
169	0.06	350	50	3	1	100	36.77	35.99	–	–	–	35.94	36.02
169	0.06	350	50	3	1	− 25	13.63	13.60	–	–	–	13.50	13.36
151	0.3	210	100	1.5	1.18	$6/(1-\nu)$	–	–	28.10	28.00	27.95	28.24	27.46
151	0.3	510	100	1.5	1.18	$6/(1-\nu)$	–	–	6.40	6.35	6.57	6.415	6.33
70	0.33	300	10	1	2	60	37.70	–	–	–	–	37.67	38.62

pull-in voltage. These results also demonstrate that, for the same material geometric parameters, pull-in voltages for nanocantilevers are lower than those of clamped–clamped nanobeams.

Next, the effect of the surface energy (surface elasticity and surface residual stress) is explored in the presence of Poisson's effect and intermolecular forces. The variations of the pull-in voltage versus the gradient index for CT, SET, MCST, and CSSE are shown in Fig. 7a for a clamped–clamped FG nanobeam. For a fixed value of the gradient index ($k = 3$), Eq. (33) is used to plot the variation of normalized maximum deflection (u) versus the applied voltage in Fig. 7b.

A further interesting study is obtained by repeating the previous case study by just changing the material length scale parameter of the upper surface of the beam (ceramic) from $l_U = 65$nm to $l_U = 10$nm, keeping $h = 3l_U$,$L = 40\ h$, $b = 5\ h$ and $d = 0.6\ h$. Thus, in this study not only the effect of the couple stress is reduced but also the dimensions of the beam are decreases and consequently the influence of intermolecular forces can be significantly observed. Results are drawn in Fig. 8. Comparing Fig. 8 with Fig. 7, the following conclusions can be derived. First, due to the smaller size of the beam, less electrostatic force is required to cause instability and hence much low pull-in voltages are observed. Second, the effect of surface energy is more significant which can be interpreted due to the increase of the surface to volume ratio. Finally, at no applied voltage, one can observe nonzero deflection in Fig. 8b compared with zero deflection in Fig. 7b. Furthermore, as the initial gap between the nanobeam and substrate becomes sufficiently small, the induced intermolecular forces cannot be neglected. These intermolecular forces induce the beam deflection even at no applied voltage. More details about influence of intermolecular forces will be considered in the following subsections.

5.2 Effect of the intermolecular forces

To clearly investigate the influence of the intermolecular forces on the pull-in voltage of actuated FG nanobeams, the nonclassical effects due to surface energy and microstructure are not incorporated, i.e. classical elasticity theory (CT) is employed. The variations of pull-in voltage versus the gradient index with and without the effects of Casimir or/and van der Waals forces are shown in Fig. 9. The dimensions of the beam are taken as $h = 10$nm, $L/h = 50$, and $b/h = 5$. Results for a clamped–clamped FG nanobeam with initial gap-to-thickness ratio $d/h = 1.2$ are plotted in Fig. 9a, whereas Fig. 9b shows results for an FG nanocantilever with $d/h = 2.6$. These results reveal that the intermolecular forces significantly reduce the pull-in voltage. Such behavior is due to that these forces increase the beam deflection and

Table 7 Comparison of the static pull-in voltage (volts) of homogeneous cantilever microactuators based on the MCST

L (μm)	$l=65$ nm			$l=592$ nm			$l=612.5$ nm		
	Rokni et al. [55]	Shaat and Mohamed [62]	Present	Rokni et al. [55]	Shaat and Mohamed [62]	Present	Rokni et al. [55]	Shaat and Mohamed [62]	Present
75	72.37	72.00	72.69	78.48	77.32	79.04	78.89	77.74	79.48
100	40.71	40.15	40.89	44.14	43.49	44.46	44.38	43.72	44.71
150	18.09	17.78	18.17	19.62	19.33	19.76	19.72	19.43	19.87
200	10.18	10.00	10.22	11.04	10.86	11.12	11.09	10.92	11.18
250	6.51	6.40	6.54	7.06	6.94	7.11	7.10	6.98	7.15

Table 8 Comparison of the static normalized pull-in tip deflection u and pull-in voltage parameter $\beta = V^2$ with the corresponding lower and upper values (u_l, u_u) and (β_l, β_u) obtained by Radi et al. [49] of a homogeneous cantilever microactuator based on the classical analysis

c_{vdW}	c_{Cas}	Neglecting fringing field				With fringing field ($d/b = 1$)			
		u (present)	(u_l, u_u) Radi et al. [49]	β (present)	(β_l, β_u) Radi et al. [49]	u (present)	(u_l, u_u) Radi et al. [49]	β (present)	(β_l, β_u) Radi et al. [49]
0	0.0	0.4484	(0.4425,0.4510)	1.6786	(1.6702,1.6965)	0.4923	(0.4864,0.4950)	1.1730	(1.1677,1.1847)
0	0.2	0.3807	(0.3812,0.3893)	1.2547	(1.2500,1.2756)	0.4042	(0.4031,0.4111)	0.8528	(0.8515,0.8680)
0	0.4	0.3363	(0.3411,0.3491)	0.8882	(0.8769,0.9023)	0.3487	(0.3539,0.3619)	0.5937	(0.5884,0.6048)
0	0.6	0.3058	(0.3101,0.3180)	0.5541	(0.5320,0.5574)	0.3120	(0.3170,0.3251)	0.3663	(0.3530,0.3695)
0	0.8	0.2832	(0.2844,0.2924)	0.2397	(0.2069,0.2323)	0.2855	(0.2869,0.2950)	0.1572	(0.1361,0.1527)
0	1.0	0.2655	(0.2623,0.2702)	− 0.0615	(− 0.103, − 0.077)	0.2649	(0.2611,0.2694)	− 0.0401	(− 0.067, − 0.051)
0.0	0	0.4484	(0.4425,0.4510)	1.6786	(1.6702,1.6965)	0.4923	(0.4864,0.4950)	1.1730	(1.1677,1.1847)
0.2	0	0.4234	(0.4183,0.4268)	1.3813	(1.3749,1.4012)	0.4572	(0.4494,0.4579)	0.9548	(0.9506,0.9677)
0.4	0	0.4003	(0.3978,0.4062)	1.0930	(1.0878,1.1142)	0.4244	(0.4198,0.4284)	0.7481	(0.7453,0.7626)
0.6	0	0.3795	(0.3797,0.3882)	0.8126	(0.8072,0.8337)	0.3955	(0.3947, 0.4033)	0.5514	(0.5489,0.5664)
0.8	0	0.3612	(0.3634,0.3719)	0.5390	(0.5321,0.5587)	0.3706	(0.3726,0.3814)	0.3631	(0.3595,0.3771)
1.0	0	0.3450	(0.3485,0.3571)	0.2712	(0.2618,0.2885)	0.3493	(0.3528,0.3617)	0.1816	(0.1758,0.1936)

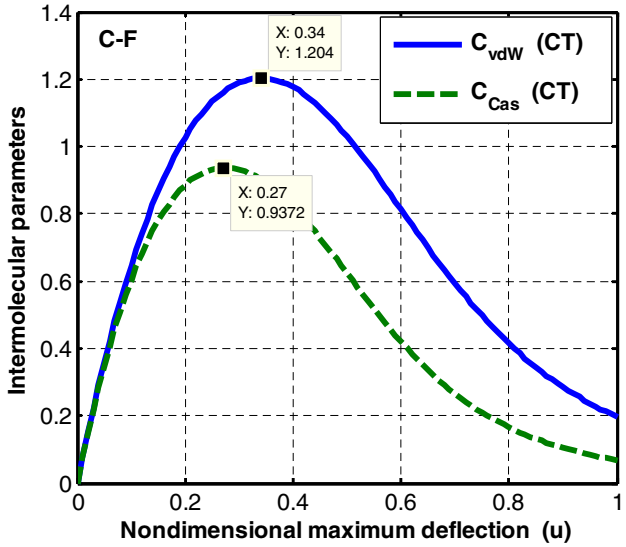

Fig. 4 Variation of intermolecular parameters c_{vdW} and c_{Cas} versus the normalized maximum deflection u for the freestanding analysis of cantilever homogeneous nanobeams based on classical analysis

consequently the pull-in instability occurs at lower applied voltage. Next, the effect of the initial gap-to-thickness ratio on the pull-in voltage with and without the intermolecular forces is demonstrated in Fig. 10 and Table 11 at $k = 1$. It is observed that the pull-in voltage significantly decreases with the decrease of d/h and that a critical value of the initial gap (d^*) exists, at which the pull-in instability occurs in the absence of any applied voltage. These situations are shown in Tables 12, 13 by symbol "-". For the geometrical and material parameters considered here, it can be observed that these critical values are $\left[d^*/h\right]_{vdW} = 0.65, \left[d^*/h\right]_{Cas} = 1.1$ for the clamped–clamped FG nanobeam and $\left[d^*/h\right]_{vdW} = 1.6$, $\left[d^*/h\right]_{Cas} = 2.3$ for the FG nanocantilever.

5.3 Freestanding nanoactuator analysis

The detachment length L^* of a nanobeam and the minimum initial gap d^* are basic design parameters for NEMS. An actuator nanobeam with specified initial gap d and length $L > L^*$ would collapse onto the substrate due to the

Table 9 Material properties of the functionally graded nanobeam constituents

Property	Upper surface, silicon [110]	Lower surface, aluminum [100]
Bulk modulus of elasticity (GPa)	$E_U = 169.2$	$E_L = 68.5$
Poisson's ratio	$\nu_U = 0.239$	$\nu_L = 0.35$
Bulk mass density $\left(\mathrm{kg/m^3}\right)$	$\rho_U = 2300$	$\rho_L = 2700$
Material couple stress length scale parameter	$l_U = 65\mathrm{nm}$	
Residual surface stress (N/m)	$\tau_U^s = 0.605$	$\tau_L^s = 0.9108$
Surface Lamé constants (N/m)	$\mu_U^s = -2.774$	$\mu_L^s = -0.376$
	$\lambda_U^s = -4.488$	$\lambda_L^s = 6.842$
Surface mass density $\left(10^7 \times \mathrm{kg/m^2}\right)$	$\rho_U^s = 3.17$	$\rho_L^s = 5.46$
Permittivity of vacuum coefficient	$\varepsilon_0 = 8.854 \times 10^{-12}\mathrm{N^{-1}m^{-2}}$	
Light speed	$\bar{c} = 2.998 \times 10^8\mathrm{m/s}$	
Hamaker constant	$\mathrm{A_H} = 2.96 \times 10^{-19}\mathrm{J}$	
Planck's constant	$h_\mathrm{P} = 1.05457 \times 10^{-34}\ \mathrm{Js}$	

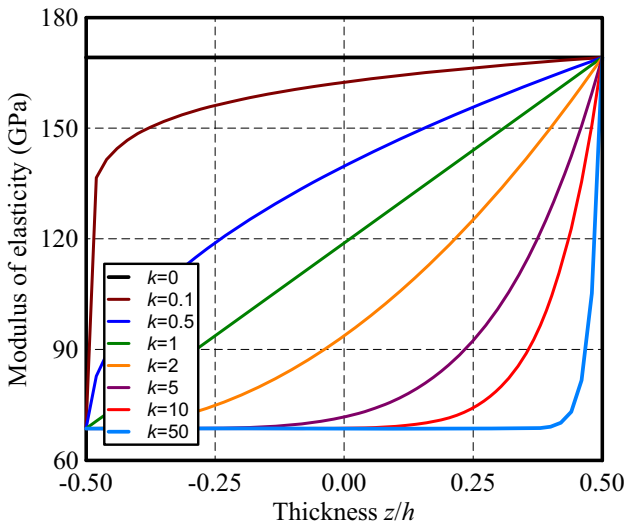

Fig. 5 Distribution of bulk Young's modulus through the thickness for different gradient index $\boldsymbol{k}$ values (Eq. (1))

intermolecular forces even in the absence of any applied voltage. If the length of the nanobeam is fixed, one can calculate the minimum gap d^* between the beam and the substrate to ensure that the nanobeam does not adhere to the substrate without applying a voltage due to the intermolecular forces. Therefore, it is very important for the designers to estimate the critical dimensions, i.e. minimum feasible gap and maximum detachment length, for the freestanding actuated FG beam to prevent collapse or adhesion due to intermolecular forces. As mentioned in Sect. 3.2, the critical points of Eqs. (39, 40) have to be computed first. Based on the values c^*_{vdW} and c^*_{Cas}, the freestanding parameters can be determined using Eqs. (41, 42). Equations (39) and (40) are plotted in Fig. 11 based on the classical elasticity and modified couple stress theories for clamped–clamped and cantilever FG nanobeams. The critical points $\left(u^*_{\mathrm{vdW}}, c^*_{\mathrm{vdW}}\right)$ and $\left(u^*_{\mathrm{Cas}}, c^*_{\mathrm{Cas}}\right)$ on the curves of Eqs. (39 and 40), respectively, are displayed in the figure. It is observed that, for both clamped–clamped and cantilever nanobeams, introducing the microstructure effect considerably increases the critical intermolecular parameters c^*_{vdW} and c^*_{Cas} but does not affect the critical normalized maximum deflections $\left(u^*_{\mathrm{Cas}}, c^*_{\mathrm{Cas}}\right)$. In addition, the predicted critical parameters under the effect of Casimir force are higher than those under the effect of van der Waals force.

Next, the critical intermolecular forces F^*_{vdW} and F^*_{Cas} are plotted versus the beam length L and initial gap d in Fig. 12. These forces are defined as

$$F^*_{\mathrm{vdW}} = \frac{c^*_{\mathrm{vdW}}}{\left(1 - u^*_{\mathrm{vdW}}\right)^3} \text{and } F^*_{\mathrm{Cas}} = \frac{c^*_{\mathrm{Cas}}}{\left(1 - u^*_{\mathrm{Cas}}\right)^4}.$$

It is observed from Fig. 12 that for a clamped–clamped FG nanobeam, the critical values of both van der Waals and Casimir forces are independent on either the beam length or the initial gap. However, these critical values depend on the material distribution (gradient index) and the microstructure material length scale parameter. Also, it can be noticed that as the stiffness of the beam increases either by decreasing k or including the couple stress effect, larger force is required to cause instability.

In Fig. 13, the minimum gap required to prevent instability of the nanoactuator due to intermolecular Casimir and van der Waals forces is plotted versus beam length in the range of 1–20 μm and thickness in the range of 6–30 nm, considering CT, MCST, and SET analyses. It is observed that, compared with MCST and SET, the classical theory

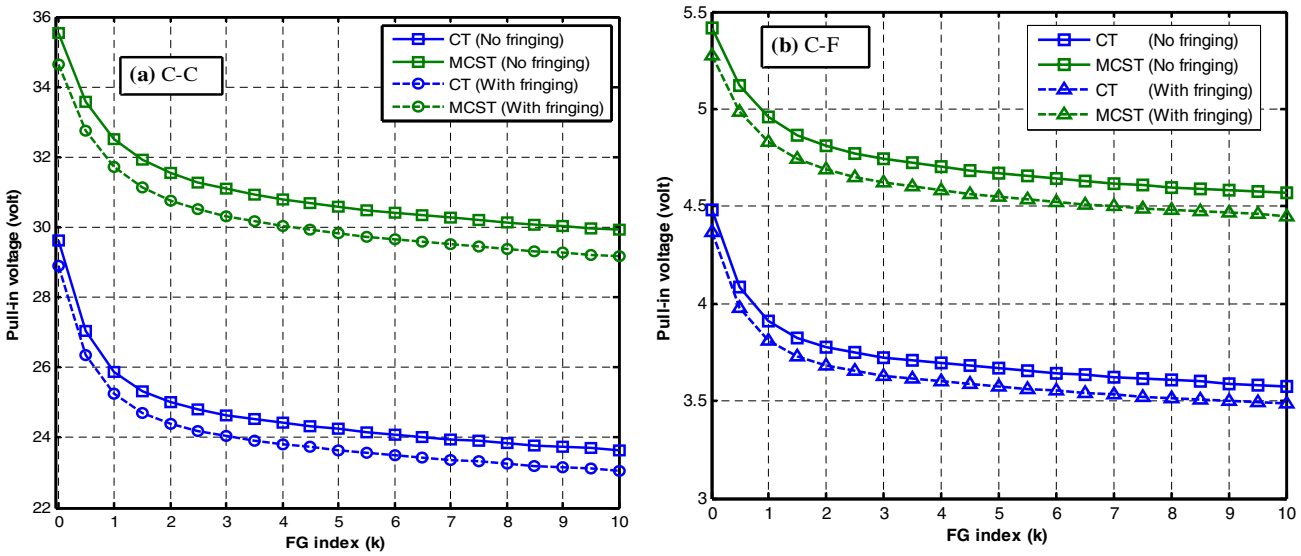

Fig. 6 Variation of the pull-in voltage of FG nanobeams versus the gradient index incorporating intermolecular forces based on the CL and MCST with and without fringing field ($l_U = 65$nm), **a** clamped–clamped and **b** cantilever FG nanobeams

Table 10 Pull-in voltages (volt) for the clamped–clamped and cantilever FG nanobeams at different gradient indices incorporating CT and MCST with and without fringing field

Gradient index k	Clamped–clamped FG nanobeam				Cantilever FG nanobeam			
	With fringing field		Without fringing field		With fringing field		Without fringing field	
	CT	MCST	CT	MCST	CT	MCST	CT	MCST
0.0 (ceramic)	28.904	34.651	29.633	35.532	4.368	5.277	4.482	5.414
0.5	26.364	32.741	27.027	33.574	3.979	4.988	4.083	5.118
1.0	25.246	31.701	25.882	32.508	3.810	4.831	3.909	4.956
5.0	23.642	29.822	24.238	30.583	3.573	4.549	3.666	4.668
10.0	23.060	29.176	23.642	29.920	3.485	4.451	3.576	4.567
∞ (metal)	21.478	27.690	22.019	28.396	3.240	4.222	3.324	4.332

CT overestimates the minimum gap which in turn lead to unexpected damage during device operation. Tables 12 and 13 tabulate the values of the minimum gap and detachment length of actuated clamped–clamped and cantilever nanobeams due to the influence of Casimir or van der Waals force based for classical and MCST analyses.

Tables 12 and 13 tabulate the values of the minimum gap and detachment length of actuated clamped–clamped and cantilever nanobeams due to the influence of Casimir or van der Waals force based for classical and MCST analyses.

6 Conclusions

A novel, simple, and accurate closed-form solution is derived for computing the size-dependent pull-in voltage of clamped–clamped and cantilever electrically actuated FG nanobeams using a Particle Swarm Optimization (PSO) algorithm. The mathematical model of the problem is presented using the size-dependent Euler–Bernoulli beam hypothesis accounting for surface energy and microstructure effects. In the present model, the modified couple-stress theory and Gurtin–Murdoch surface elasticity model are employed to, respectively, determine the effect of microstructure local rotational degree of freedom and surface energy effect on the pull-in behavior of FG micro/nanobeam. The model accounts for the simultaneous effect of intermolecular Casimir and van der Waals forces, fringing field, mid-plane stretching, and axial residual stress. All properties of the bulk material and surface layers of the FG beam are supposed to vary across the thickness direction according to power-law. The governing equation and boundary conditions are exactly derived employing Hamilton principle accounting for the position of physical neutral axis of the mentioned FG nanobeam.

Using Galerkin method, the governing equation is reduced to an algebraic-integral equation, then a PSO method is utilized to approximate the integral forms of the

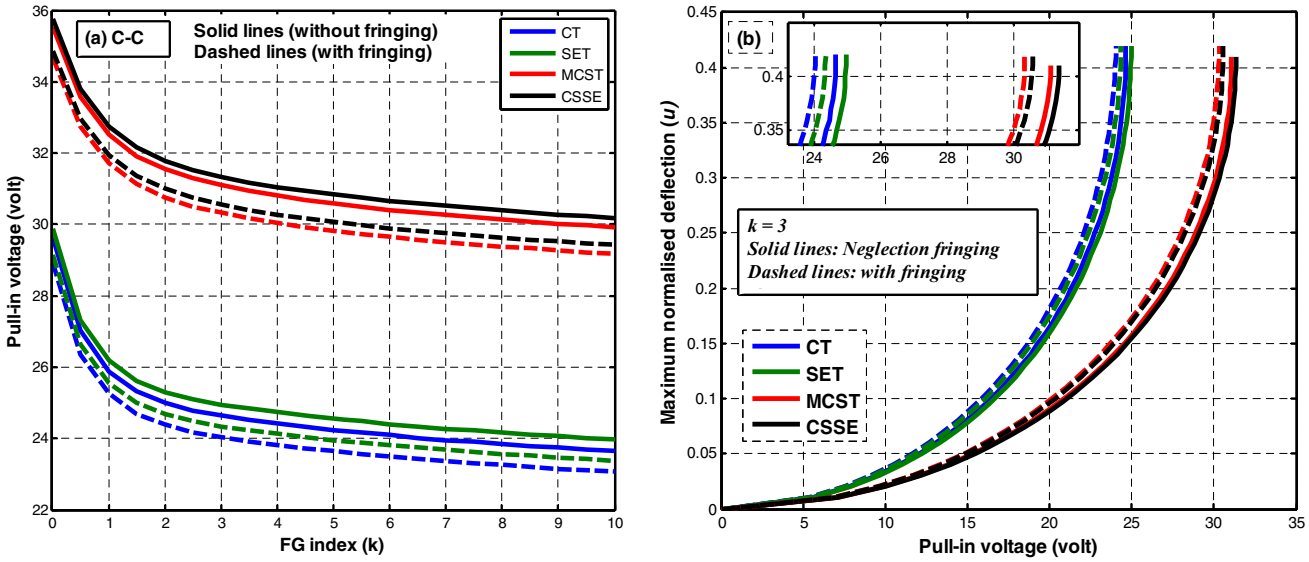

Fig. 7 Pull-in behavior of a clamped–clamped FG nanobeam with and without fringing field for CT, SET, MCST, and CSSE analyses ($l_U = 65$nm), **a** variation of the pull-in voltage versus the gradient index and **b** variation of normalized maximum deflection versus the applied voltage at $k = 3$

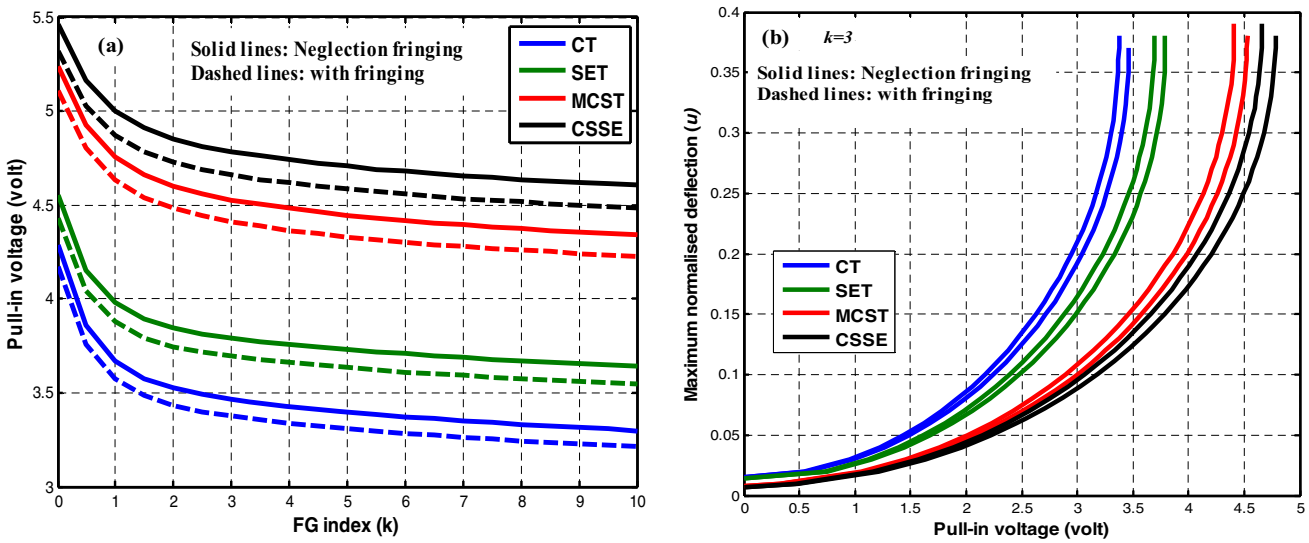

Fig. 8 Pull-in behavior of a clamped–clamped FG nanobeam with and without fringing field for CT, SET, MCST, and CSSE analyses ($l_U = 10$nm) **a** variation of the pull-in voltage with the gradient index and **b** variation of normalized maximum deflection with the applied voltage at $k = 3$

fringing field, electrostatic, and intermolecular Casimir and van der Waals forces to non-integral forms. Finally, a general closed form solution of the pull-in voltage is obtained. Also, the proposed method leads to an accurate prediction of the detachment length and minimum initial gap of the freestanding nanoactuator. The main conclusions that can be extracted from the numerical results are outlined as follows:

1. Different coefficients of the non-integral forms for electrostatic force, fringing field effect, and intermolecular Casimir and van der Waals forces are extracted using PSO and tabulated (Tables 2, 3).
2. A single nonlinear algebraic equation (Eq. (33)) is derived for the relation between the applied voltage and the maximum normalized deflection of the FG nanoactuator. This equation is very helpful for understanding the instability behavior under the mutual nonlinear

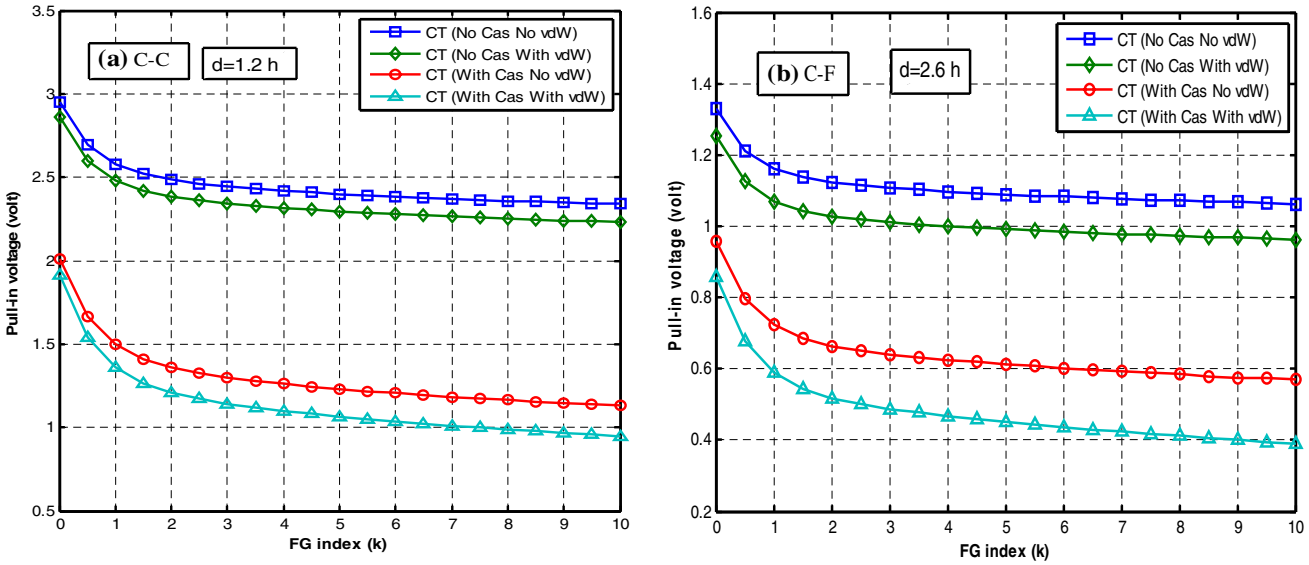

Fig. 9 Variation of the pull-in voltage versus the gradient index based on the classical elasticity theory with and without the Casimir and van der Waals forces, **a** clamped–clamped **b** cantilever nanobeams

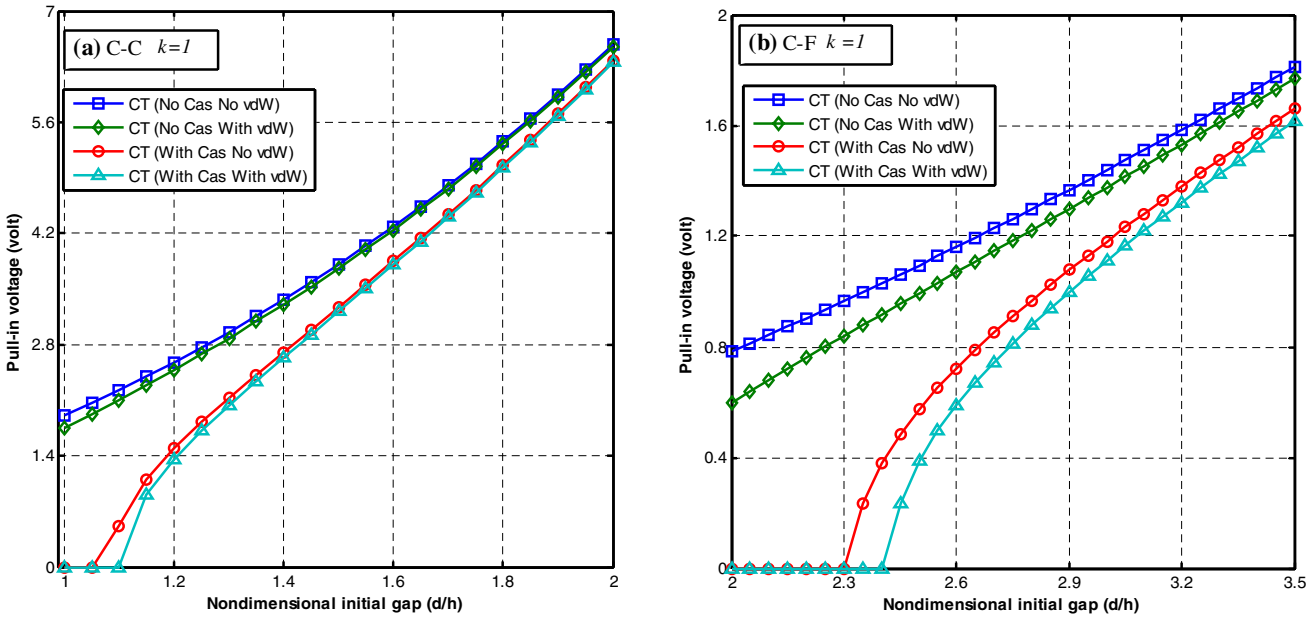

Fig. 10 Variation of the pull-in voltage versus the initial gap-to-thickness ratio d/h based on the classical elasticity theory with and without the Casimir and van der Waals forces ($k = 1$), **a** clamped–clamped, **b** cantilever nanobeams

effects of mechanical, electrostatic, and intermolecular forces. Based on this equation, the closed-form expressions for pull-in voltage and freestanding parameters are easily derived. Besides being simple, the accuracy of the closed-form expression for pull-in voltage of micro/nanobeams with clamped–clamped and clamped-free boundary conditions as well as the detachment length and minimum gap of the freestanding nanoactuator are verified by comparing the present results with those in published literature and good agreement is found.

3. The presence of surface energy effects (surface elasticity and surface residual stress) leads to a higher pull-in voltage compared with that of classical theory due to the stiffening effect of surface modulus. The effects

Table 11 Pull-in voltage (volt) at different gap-to-thickness ratios d/h for clamped–clamped and cantilever FG nanobeams based on the classical elasticity theory with and without (WO) the intermolecular forces ($k = 1$)

Clamped–clamped FG nanobeam					Cantilever FG nanobeam				
d/h	WO	vdW	Cas	vdW and Cas	d/h	WO	vdW	Cas	vdW and Cas
0.5	0.642	–	–	–	1.0	0.277	–	–	–
0.65	0.962	0.377	–	–	1.55	0.534	–	–	–
1.0	1.905	1.748	–	–	1.60	0.560	0.072	–	–
1.1	2.229	2.106	0.518	–	2.30	0.966	0.840	–	–
1.2	2.580	2.482	1.495	1.360	2.35	0.998	0.878	0.234	–
1.5	3.813	3.758	3.274	3.216	2.40	1.030	0.917	0.380	–
2.0	6.581	6.556	6.381	6.355	2.50	1.095	0.994	0.573	0.389

Table 12 Minimum gap (nm) due to Casimir or van der Waals force at different beam lengths for clamped–clamped and cantilever nanobeams ($k = 0$, $b = h = 10$ nm)

L (μm)	Clamped–clamped nanobeam				Cantilever nanobeam			
	CT		MCST		CT		MCST	
	d^*_{vdW}	d^*_{Cas}	d^*_{vdW}	d^*_{Cas}	d^*_{vdW}	d^*_{Cas}	d^*_{vdW}	d^*_{Cas}
1	12.213	18.835	10.016	16.071	31.014	39.682	25.435	33.860
5	61.066	68.255	50.080	58.241	155.072	143.802	127.175	122.704
10	122.131	118.839	100.160	101.404	310.143	250.374	254.350	213.641
15	183.197	164.373	150.241	140.258	465.215	346.307	381.525	295.500
20	244.262	206.910	200.321	176.554	620.286	435.926	508.700	371.970
25	305.328	247.349	250.401	211.060	775.358	521.123	635.875	444.668
30	366.394	286.190	300.481	244.203	930.430	602.956	763.051	514.495

Table 13 Detachment length (μm) due to Casimir or van der Waals force at different initial gaps for clamped–clamped and cantilever nanobeams ($k = 0$, $b = h = 10$ nm)

d(nm)	Clamped–clamped nanobeam				Cantilever nanobeam			
	CT		MCST		CT		MCST	
	L^*_{vdW}	L^*_{Cas}	L^*_{vdW}	L^*_{Cas}	L^*_{vdW}	L^*_{Cas}	L^*_{vdW}	L^*_{Cas}
10	0.819	0.453	0.998	0.553	0.322	0.179	0.393	0.218
50	4.094	3.389	4.992	4.132	1.612	1.335	1.966	1.628
100	8.188	8.059	9.984	9.827	3.224	3.175	3.932	3.872
150	12.282	13.379	14.976	16.313	4.836	5.271	5.897	6.427
200	16.376	19.169	19.968	23.373	6.449	7.552	7.863	9.208

of surface energy become considerable when the beam reduced to nanoscale. Comparison between CT, MCST, SET, and CSSE demonstrates that the nonclassical analyses predict higher pull-in voltage due to the stiffness effect, which becomes stronger in CSSE than SET and MCST.

4. For both classical and nonclassical analyses, increasing the gradient index shows a significant reduction in the pull-in voltage. This is attributed to the softening effect as the gradient index increases, since we assume that the constitution of ceramic in the material decreases with increasing k.
5. The coupled effects of fringing field and intermolecular Casimir and van der Waals forces distinctly decrease the pull-in voltage. If the contribution of these effects is neglected, the pull-in voltage may be considerably overestimated leading to unexpected damage during device operation. Therefore, the present investigation may be very helpful for assuring the safe operation of MEMS and NEMS actuators. As the initial gap decreases, the influence of the intermolecular forces become more significant and the nanobeam may collapse at no applied voltage.
6. The proposed method is used to determine the critical dimensions of the freestanding FG nanoactuators, i.e. minimum initial gap and detachment length. It is observed that the critical intermolecular forces are independent of the beam length and the initial gap. Increasing the gradient index, smaller forces are required to cause pull-in. In addition, neglecting the nonclassical

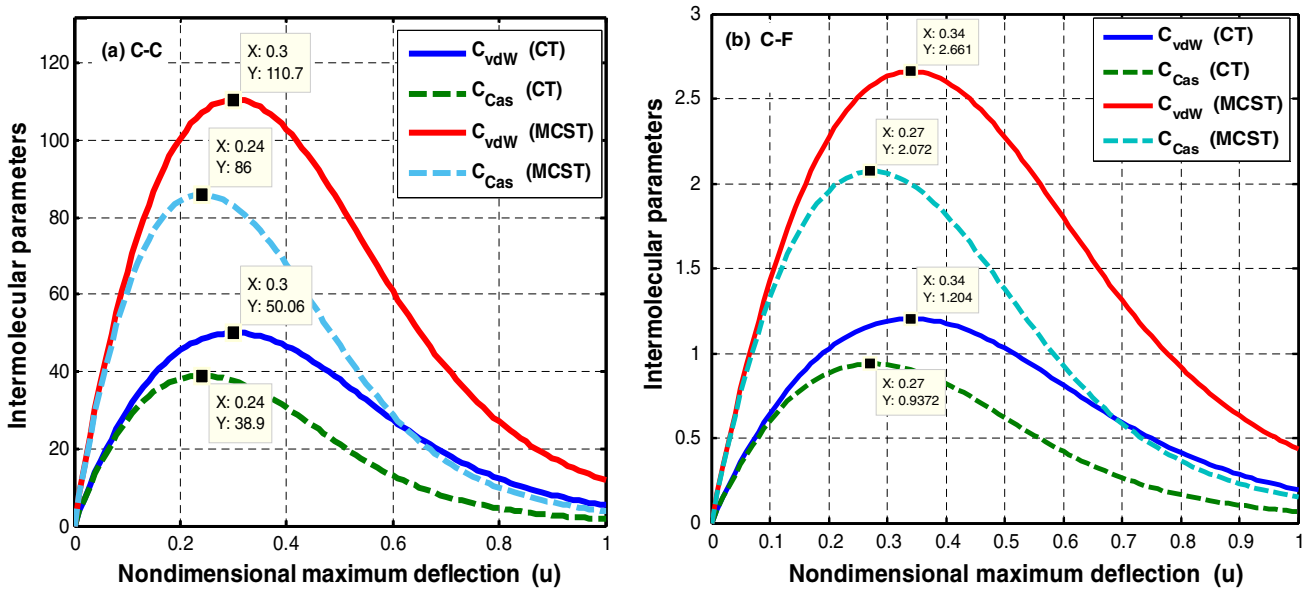

Fig. 11 Variation of intermolecular parameters c_{vdW} and c_{Cas} versus the normalized maximum deflection for the freestanding analysis ($k = 0$), **a** clamped–clamped (neglecting mid-stretching) and **b** cantilever homogeneous nanobeams

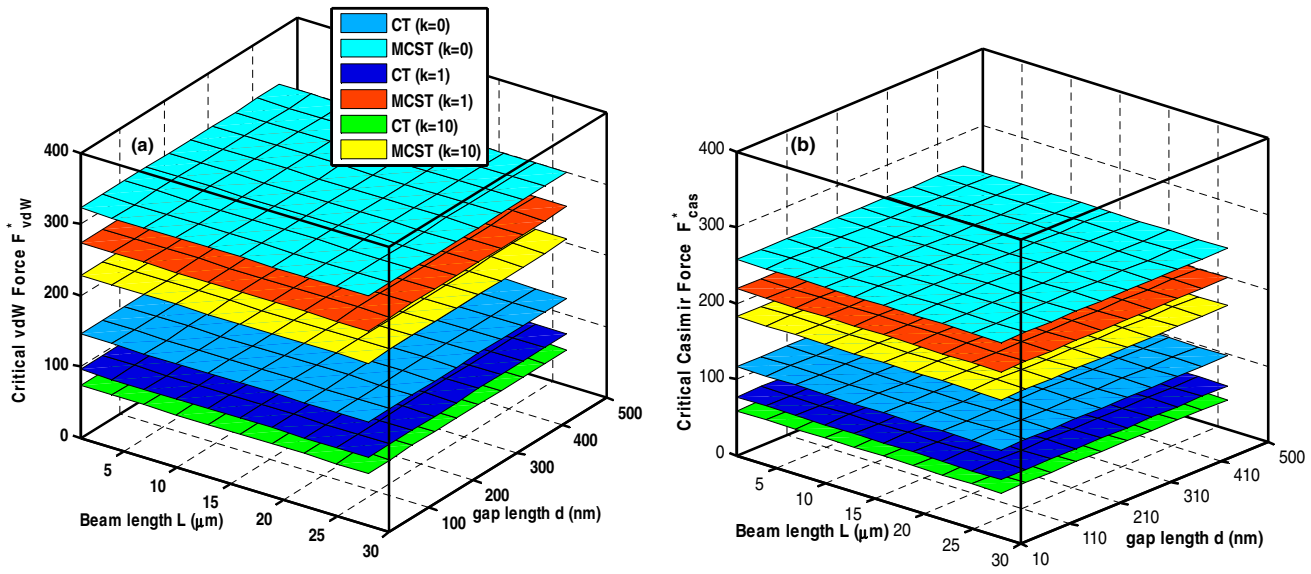

Fig. 12 Variation of critical intermolecular forces versus beam length and initial gap length based on CT and MCST analysis for different gradient indices of clamped–clamped FG nanoactuator ($h = 10\mathrm{nm}, b = 5h, l_U = 0.5h, l_B = 0.75h$), **a** critical van der Waals and **b** critical Casimir force

effects overestimates the minimum gap which may result in unexpected damage of the actuator if it is designed based on classical theory.

This present model and the proposed analytical solution can be used as an efficient accurate tool for predicting the influences of the material and geometrical parameters on the size-dependent static pull-in instability and freestanding behavior of FG nanobeams for their design and optimization which may need a large number of simulations.

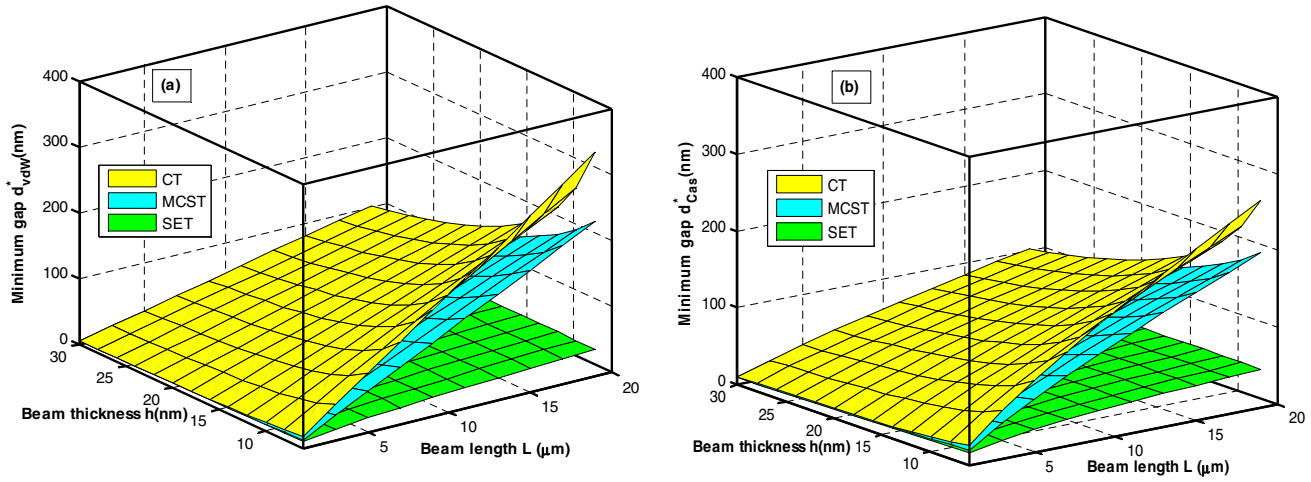

Fig. 13 Variation of minimum gap for **a** van der Walls and **b** Casimir forces versus beam length and thickness for CT and MCST and SET analyses of a clamped–clamped FG nanoactuator, ($k = 0, b = 50$nm, $l_U = 5$nm), **a** due to van der Waals force only and **b** due to Casimir force only

References

1. Abdi J, Koochi A, Kazemi AS, Abadyan M (2011) Modeling the effects of size dependence and dispersion forces on the pull-in instability of electrostatic cantilever NEMS using modified couple stress theory. Smart Mater Struct 20(5):055011
2. Attia MA (2017) Investigation of size-dependent quasistatic response of electrically actuated nonlinear viscoelastic microcantilevers and microbridges. Meccanica 52(10):2391–2420
3. Attia MA (2017) On the mechanics of functionally graded nanobeams with the account of surface elasticity. Int J Eng Sci 115:73–101
4. Attia MA, Emam SA (2018) Electrostatic nonlinear bending, buckling and free vibrations of viscoelastic microbeams based on the modified couple stress theory. Acta Mech 229(8):3235–3255
5. Attia MA, Mahmoud FF (2016) Modeling and analysis of nanobeams based on nonlocal-couple stress elasticity and surface energy theories. Int J Mech Sci 105:126–134
6. Attia MA, Mohamed SA (2017) Nonlinear modeling and analysis of electrically actuated viscoelastic microbeams based on the modified couple stress theory. Appl Math Model 41:195–222
7. Attia MA, Mohamed SA (2018) Pull-in instability of functionally graded cantilever nanoactuators incorporating effects of microstructure, surface energy and intermolecular forces. Int J Appl Mech 10(08):1850091
8. Attia MA, Mohamed SA (2020) Nonlinear thermal buckling and postbuckling analysis of bidirectional functionally graded tapered microbeams based on Reddy beam theory. Eng Comput. https://doi.org/10.1007/s00366-020-01080-1
9. Attia MA, Rahman AAA (2018) On vibrations of functionally graded viscoelastic nanobeams with surface effects. Int J Eng Sci 127:1–32
10. Attia MA, Shanab RA, Mohamed SA, Mohamed NA (2019) Surface energy effects on the nonlinear free vibration of functionally graded Timoshenko nanobeams based on modified couple stress theory. Int J Struct Stab Dyn 19(11):1950127
11. Baghani M (2012) Analytical study on size-dependent static pull-in voltage of microcantilevers using the modified couple stress theory. Int J Eng Sci 54:99–105
12. Ballestra A, Brusa E, Munteanu MG, Somà A (2008) Experimental characterization of electrostatically actuated in-plane bending of microcantilevers. Microsyst Technol 14(7):909–918
13. Batra RC, Porfiri M, Spinello D (2008) Effects of van der Waals force and thermal stresses on pull-in instability of clamped rectangular microplates. Sensors 8(2):1048–1069
14. Bhojawala VM, Vakharia DP (2017) Closed-form relation to predict static pull-in voltage of an electrostatically actuated clamped–clamped microbeam under the effect of Casimir force. Acta Mech 228(7):2583–2602
15. Bochobza-Degani O, Nemirovsky Y (2002) Modeling the pull-in parameters of electrostatic actuators with a novel lumped two degrees of freedom pull-in model. Sens Actuators A 97:569–578
16. Chowdhury S, Ahmadi M, Miller WC (2005) A closed-form model for the pull-in voltage of electrostatically actuated cantilever beams. J Micromech Microeng 15(4):756
17. Dehghan M, Ebrahimi F, Vinyas M (2019) Wave dispersion characteristics of fluid-conveying magneto-electro-elastic nanotubes. Eng Comput:1–17
18. Duan J, Li Z, Liu J (2016) Pull-in instability analyses for NEMS actuators with quartic shape approximation. Appl Math Mech 37(3):303–314
19. Eberhart RC, Shi Y, Kennedy J (2001) Swarm intelligence. Elsevier, Oxford
20. Ebrahimi F, Hosseini SHS (2019) Nonlinear vibration and dynamic instability analysis nanobeams under thermo-magneto-mechanical loads: a parametric excitation study. Eng Comput:1–14
21. Ebrahimi F, Hosseini SHS (2020) Effect of residual surface stress on parametrically excited nonlinear dynamics and instability of double-walled nanobeams: an analytical study. Eng Comput:1–12
22. Ebrahimi F, Karimiasl M, Singhal A (2019) Magneto-electro-elastic analysis of piezoelectric–flexoelectric nanobeams rested on silica aerogel foundation. Eng Comput:1–8
23. Eltaher MA, Alshorbagy AE, Mahmoud FF (2013) Determination of neutral axis position and its effect on natural frequencies of functionally graded macro/nanobeams. Compos Struct 99:193–201
24. Eltaher MA, Abdelrahman AA, Al-Nabawy A, Khater M, Mansour A (2014) Vibration of nonlinear graduation of nano-Timoshenko beam considering the neutral axis position. Appl Math Comput 235:512–529

25. Fan F, Lei B, Sahmani S, Safaei B (2020) On the surface elastic-based shear buckling characteristics of functionally graded composite skew nanoplates. Thin Wall Struct 154:106841
26. Farrokhabadi A, Mohebshahedin A, Rach R, Duan JS (2016) An improved model for the cantilever NEMS actuator including the surface energy, fringing field and Casimir effects. Phys E 75:202–209
27. Fattahi AM, Sahmani S, Ahmed NA (2019) Nonlocal strain gradient beam model for nonlinear secondary resonance analysis of functionally graded porous micro/nano-beams under periodic hard excitations. Mech Based Des Struct Mach:1–30
28. Gao XL (2015) A new Timoshenko beam model incorporating microstructure and surface energy effects. Acta Mech 226(2):457–474
29. Gao XL, Mahmoud FF (2014) A new Bernoulli–Euler beam model incorporating microstructure and surface energy effects. Zeitschrift für angewandte Mathematik und Physik 65(2):393–404
30. Gao XL, Zhang GY (2016) A non-classical Kirchhoff plate model incorporating microstructure, surface energy and foundation effects. Continuum Mech Thermodyn 28(1–2):195–213
31. Gurtin ME, Murdoch AI (1975) A continuum theory of elastic material surfaces. Arch Ration Mech Anal 57(4):291–323
32. Gurtin ME, Murdoch AI (1978) Surface stress in solids. Int J Solids Struct 14(6):431–440
33. Haluzan DT, Klymyshyn DM, Achenbach S, Börner M (2010) Reducing pull-in voltage by adjusting gap shape in electrostatically actuated cantilever and fixed-fixed beams. Micromachines 1(2):68–81
34. Hu YC, Chang CM, Huang SC (2004) Some design considerations on the electrostatically actuated microstructures. Sens Actuators A 112(1):155–161
35. Kennedy J, Eberhart R (1995) Particle swarm optimization. In: Proceedings of ICNN'95-international conference on neural networks. IEEE, vol 4, pp 1942–1948
36. Kuang JH, Chen CJ (2004) Dynamic characteristics of shaped micro-actuators solved using the differential quadrature method. J Micromech Microeng 14(4):647
37. Liu H, Lyu Z (2020) Modeling of novel nanoscale mass sensor made of smart FG magneto-electro-elastic nanofilm integrated with graphene layers. Thin Wall Struct 151:106749
38. Liu H, Wu H, Lyu Z (2020) Nonlinear resonance of FG multilayer beam-type nanocomposites: effects of graphene nanoplatelet-reinforcement and geometric imperfection. Aerosp Sci Technol 98:105702
39. Lyu Z, Yang Y, Liu H (2020) High-accuracy hull iteration method for uncertainty propagation in fluid-conveying carbon nanotube system under multi-physical fields. Appl Math Model 79:362–380
40. Ma Y, Gao Y, Yang W, He D (2020) Free vibration of a micro-scale composite laminated Reddy plate using a finite element method based on the new modified couple stress theory. Res Phys 16:102903
41. Mahmoud FF, Eltaher MA, Alshorbagy AE, Meletis EI (2012) Static analysis of nanobeams including surface effects by nonlocal finite element. J Mech Sci Technol 26(11):3555–3563
42. Miandoab EM, Pishkenari HN, Meghdari A, Fathi M (2017) A general closed-form solution for the static pull-in voltages of electrostatically actuated MEMS/NEMS. Phys E 90:7–12
43. Miller RE, Shenoy VB (2000) Size-dependent elastic properties of nanosized structural elements. Nanotechnology 11(3):139
44. Nayfeh AH, Younis MI, Abdel-Rahman EM (2005) Reduced-order models for MEMS applications. Nonlinear Dyn 41(1–3):211–236
45. O'Mahony C, Hill M, Duane R, Mathewson A (2003) Analysis of electromechanical boundary effects on the pull-in of micromachined fixed–fixed beams. J Micromech Microeng 13(4):S75
46. Osterberg PM, Senturia SD (1997) M-TEST: a test chip for MEMS material property measurement using electrostatically actuated test structures. J Microelectromech Syst 6(2):107–118
47. Ouakad HM, Sedighi HM, Younis MI (2017) One-to-one and three-to-one internal resonances in MEMS shallow arches. J Comput Nonlinear Dyn 12(5):051025
48. Pamidighantam S, Puers R, Baert K, Tilmans HA (2002) Pull-in voltage analysis of electrostatically actuated beam structures with fixed–fixed and fixed–free end conditions. J Micromech Microeng 12(4):458
49. Radi E, Bianchi G, di Ruvo L (2017) Upper and lower bounds for the pull-in parameters of a micro-or nanocantilever on a flexible support. Int J Non-Linear Mech 92:176–186
50. Radi E, Bianchi G, di Ruvo L (2018) Analytical bounds for the electromechanical buckling of a compressed nanocantilever. Appl Math Model 59:571–582
51. Rahaeifard M, Kahrobaiyan MH, Asghari M, Ahmadian MT (2011) Static pull-in analysis of microcantilevers based on the modified couple stress theory. Sens Actuators A 171(2):370–374
52. Ramezani A, Alasty A, Akbari J (2007) Closed-form solutions of the pull-in instability in nano-cantilevers under electrostatic and intermolecular surface forces. Int J Solids Struct 44(14–15):4925–4941
53. Ramezani A, Alasty A, Akbari J (2007) Closed-form approximation and numerical validation of the influence of van der Waals force on electrostatic cantilevers at nano-scale separations. Nanotechnology 19(1):015501
54. Rhoads JF, Shaw SW, Turner KL (2006) The nonlinear response of resonant microbeam systems with purely-parametric electrostatic actuation. J Micromech Microeng 16(5):890
55. Rokni H, Seethaler RJ, Milani AS, Hosseini-Hashemi S, Li XF (2013) Analytical closed-form solutions for size-dependent static pull-in behavior in electrostatic micro-actuators via Fredholm integral equation. Sens Actuators A 190:32–43
56. Sadeghian H, Rezazadeh G, Osterberg PM (2007) Application of the generalized differential quadrature method to the study of pull-in phenomena of MEMS switches. J Microelectromech Syst 16(6):1334–1340
57. Sahmani S, Safaei B (2020) Influence of homogenization models on size-dependent nonlinear bending and postbuckling of bi-directional functionally graded micro/nano-beams. Appl Math Model 82:336–358
58. Sahmani S, Fattahi AM, Ahmed NA (2019) Analytical mathematical solution for vibrational response of postbuckled laminated FG-GPLRC nonlocal strain gradient micro-/nanobeams. Eng Comput 35(4):1173–1189
59. Sedighi HM (2014) The influence of small scale on the pull-in behavior of nonlocal nanobridges considering surface effect, Casimir and Van der Waals attractions. Int J Appl Mech 6(03):1450030
60. Sedighi HM (2014) Size-dependent dynamic pull-in instability of vibrating electrically actuated microbeams based on the strain gradient elasticity theory. Acta Astronaut 95:111–123
61. Sedighi HM, Daneshmand F, Abadyan M (2016) Modeling the effects of material properties on the pull-in instability of nonlocal functionally graded nano-actuators. ZAMM J Appl Math Mech 96(3):385–400
62. Shaat M, Mohamed SA (2014) Nonlinear-electrostatic analysis of micro-actuated beams based on couple stress and surface elasticity theories. Int J Mech Sci 84:208–217
63. Shaat M, Mahmoud FF, Gao XL, Faheem AF (2014) Size-dependent bending analysis of Kirchhoff nano-plates based on a modified couple-stress theory including surface effects. Int J Mech Sci 79:31–37
64. Shams Alizadeh M, Heidari Shirazi K, Moradi S, Sedighi HM (2018) Numerical analysis of the counter-intuitive dynamic

behavior of the elastic-plastic pin-ended beams under impulsive loading with regard to linear hardening effects. Proc Inst Mech Eng Part C J Mech Eng Sci 232(24):4588–4600
65. Shanab RA, Mohamed SA, Mohamed NA, Attia MA (2020a) Comprehensive investigation of vibration of sigmoid and power law FG nanobeams based on surface elasticity and modified couple stress theories. Acta Mech:1–34
66. Shanab RA, Attia MA, Mohamed SA (2017) Nonlinear analysis of functionally graded nanoscale beams incorporating the surface energy and microstructure effects. Int J Mech Sci 131:908–923
67. Shanab RA, Attia MA, Mohamed SA, Mohamed NA (2020) Effect of microstructure and surface energy on the static and dynamic characteristics of FG Timoshenko nanobeam embedded in an elastic medium. J Nano Res 61:97–117
68. Shenoy VB (2005) Atomistic calculations of elastic properties of metallic fcc crystal surfaces. Phys Rev B 71(9):094104
69. Soroush R, Koochi A, Kazemi AS, Noghrehabadi A, Haddadpour H, Abadyan M (2010) Investigating the effect of Casimir and van der Waals attractions on the electrostatic pull-in instability of nano-actuators. Phys Scr 82(4):045801
70. Tahani M, Askari AR (2014) Accurate electrostatic and van der Waals pull-in prediction for fully clamped nano/microbeams using linear universal graphs of pull-in instability. Phys E 63:151–159
71. Thanh CL, Tran LV, Vu-Huu T, Abdel-Wahab M (2019) The size-dependent thermal bending and buckling analyses of composite laminate microplate based on new modified couple stress theory and isogeometric analysis. Comput Methods Appl Mech Eng 350:337–361
72. Tilmans HA, Legtenberg R (1994) Electrostatically driven vacuum-encapsulated polysilicon resonators: Part. II Theory and performance. Sens Actuators A Phys 45(1):67–84
73. Trinh LC, Groh RM, Zucco G, Weaver PM (2020) A strain-displacement mixed formulation based on the modified couple stress theory for the flexural behaviour of laminated beams. Compos B Eng 185:107740
74. Wang B, Zhou S, Zhao J, Chen X (2011) Size-dependent pull-in instability of electrostatically actuated microbeam-based MEMS. J Micromech Microeng 21(2):027001
75. Wang KF, Kitamura T, Wang B (2015) Nonlinear pull-in instability and free vibration of micro/nanoscale plates with surface energy–a modified couple stress theory model. Int J Mech Sci 99:288–296
76. Wu H, Liu H (2020) Nonlinear thermo-mechanical response of temperature-dependent FG sandwich nanobeams with geometric imperfection. Eng Comput:1–21
77. Xie B, Sahmani S, Safaei B, Xu B (2020) Nonlinear secondary resonance of FG porous silicon nanobeams under periodic hard excitations based on surface elasticity theory. Eng Comput:1–24
78. Yang FACM, Chong ACM, Lam DCC, Tong P (2002) Couple stress based strain gradient theory for elasticity. Int J Solids Struct 39(10):2731–2743
79. Yi H, Sahmani S, Safaei B (2020) On size-dependent large-amplitude free oscillations of FGPM nanoshells incorporating vibrational mode interactions. Arch Civ Mech Eng 20:1–23
80. Yin L, Qian Q, Wang L (2011) Size effect on the static behavior of electrostatically actuated microbeams. Acta Mech Sin 27(3):445
81. Younis MI (2011) MEMS linear and nonlinear statics and dynamics, vol 20. Springer, Berlin
82. Younis MI, Abdel-Rahman EM, Nayfeh A (2003) A reduced-order model for electrically actuated microbeam-based MEMS. J Microelectromech Syst 12(5):672–680
83. Yuan Y, Zhao K, Sahmani S, Safaei B (2020) Size-dependent shear buckling response of FGM skew nanoplates modeled via different homogenization schemes. Appl Math Mech:1–18
84. Yuan Y, Zhao K, Zhao Y, Sahmani S, Safaei B (2020) Couple stress-based nonlinear buckling analysis of hydrostatic pressurized functionally graded composite conical microshells. Mech Mater:103507
85. Yuan Y, Zhao K, Han Y, Sahmani S, Safaei B (2020) Nonlinear oscillations of composite conical microshells with in-plane heterogeneity based upon a couple stress-based shell model. Thin Wall Struct 154:106857
86. Zhang G, Gao XL (2019) Elastic wave propagation in a periodic composite plate structure: band gaps incorporating microstructure, surface energy and foundation effects. J Mech Mater Struct 14(2):219–236
87. Zhang Q, Liu H (2020) On the dynamic response of porous functionally graded microbeam under moving load. Int J Eng Sci 153:103317
88. Zhang LX, Zhao YP (2003) Electromechanical model of RF MEMS switches. Microsyst Technol 9(6–7):420–426